CO_2 Storage in a Devonian Carbonate System, Fort Nelson British Columbia

by

Peter W. Crockford
BSc., University of Victoria, 2008

A Thesis Submitted in Partial Fulfillment
of the Requirements for the Degree of

MASTER OF SCIENCE

in the School of Earth and Ocean Sciences

Supervisory Committee

CO_2 Storage in a Devonian Carbonate System, Fort Nelson British Columbia

by

Peter W. Crockford

B.Sc. University of Victoria, 2008

Supervisory Committee

Dr. Kevin Telmer (School of Earth and Ocean Sciences)
Supervisor

Dr. Melvin Best (School of Earth and Ocean Sciences)
Departmental Member

Dr. Dante Canil (School of Earth and Ocean Sciences)
Departmental Member

Abstract

Supervisory Committee
Dr. Kevin Telmer (School of Earth and Ocean Sciences)
Supervisor
Dr. Melvin Best (School of Earth and Ocean Sciences)
Departmental Member
Dr. Dante Canil (School of Earth and Ocean Sciences)
Departmental Member

This study geochemically characterized a proposed Carbon Capture and Storage project in northeast British Columbia, and presents new dissolution kinetics data for the proposed saline aquifer storage reservoir, the Keg River Formation. The Keg River Formation is a carbonate reservoir (89-93% Dolomite, 5-8% Calcite) at approximately 2200 m depth, at a pressure of 190 bar, and temperature of 105 °C. The Keg River brine is composed of Na, Cl, Ca, K, Mg, S, Si, and HCO_3 and is of approximately 0.4 M ionic strength. Fluid analysis found the Keg River brine to be relatively fresh compared with waters of the Keg River formation in Alberta, and to also be distinct from waters in overlying units. These findings along with the physical conditions of the reservoir make the Keg River Formation a strong candidate for CO_2 storage.

Further work measured the dissolution rates of Keg River rock that will occur within the Keg River formation. This was performed in a new experimental apparatus at 105 °C, and 50 bar pCO_2 with brine and rock sampled directly from the reservoir. Dissolution rate constants ($mol \cdot m^{-2}s^{-1}$) for Keg River rock were found to be Log K_{Mg} 9.80 ±.02 and Log K_{Ca} -9.29 ±.04 for the Keg River formation. These values were found to be significantly lower compared to rate constants generated from experiments involving synthetic brines with values of Log K_{Mg} -9.43 ±.09, and Log K_{Ca} -9.23 ±.21. Differences in rates were posited as due to influences of other element interactions with the >MgOH hydration site, which was tested through experiments with brines spiked with $SrCl_2$ and $ZnCl_2$. Results for the $SrCl_2$ spiked solution showed little impact on dissolution rates with rate constants of Log K_{Mg} -9.43 ±.09, and Log K_{Ca} -9.15 ±.21, however the $ZnCl_2$ spiked solution did show some inhibition with rate constants of Log K_{Mg} -9.67 ±.04, and Log K_{Ca} -9.30 ±.04. Rate constants generated in this work are among the first presented which can actually be tested by full-scale injection of CO_2.

Table of Contents

List of Tables

List of Figures

Acknowledgments

This work would not have been possible without the ongoing academic and financial support of my Supervisors Dr. Kevin Telmer, and Dr. Melvin Best. I would like to offer my sincere thanks for their advice and guidance both related and unrelated to this work. I would also like to thank the government of British Columbia Ministry of Energy, Mines, and Petroleum Resources, and the University of Victoria School of Earth and Ocean Sciences who provided the funding for this work.

Thank you to Ricardo Rosin for his support in the lab and thanks to Jamie Macgregor for technical support, and keeping me sane through this whole process. Thank you to Vic Levson and Alf Hartling from the Ministry of Energy, Mines, and Petroleum Resources for information on the project and inclusion in meetings. This work would not have been possible without access to the field location provided by Dave Moffatt and Spectra Energy.

Many thanks to the University of Victoria School of Earth and Ocean Science for cultivating me into a geoscientist. I would like to offer particular acknowledgement to Dr. Jay Cullen, Dr. Dante Canil, and Dr. Stephen Johnston for providing me with inspiring courses, which have played integral roles in my aspirations in studying the Earth.

Finally thanks to my wonderful friends Lindsay Walton, Devin Tait, Devin Stark and Evan Riddell for fun whenever I had free time, and to my family Devi, Dennis and John Crockford and my girlfriend Lindsay Walton, your continued love and support will always be cherished.

Dedication

For Dennis and Devi

Chapter 1: Introduction

1.1 Anthropogenic Climate Change

In its fourth assessment the Intergovernmental Panel on Climate Change (IPCC) asserted that increases in global mean temperature are "very likely" attributed to anthropogenic emissions of greenhouse gases (GHG) (Solomon, 2007). The GHG receiving the greatest amount of attention and concern from scientists is CO_2, which is predominantly produced through the combustion of fossil fuels. As of the year 2000, an estimated 65% of total global CO_2 emissions (30 Gtons) is generated within the energy sector which includes: transport, electricity, and heat generation (Baumert et al., 2005). In order to make significant CO_2 reductions, the energy sector is the most effective place to start (IEAGHG, 2008).

A rise in global mean temperature has experts concerned because this stresses fragile ecosystems, and many of the most impoverished people on the planet (Patz, 2005). Some predicted outcomes in a warmer world include drought, floods, water shortages, and increased sea level (Parry, 2007). Citizens of wealthy nations have the ability to migrate, however large amounts of our infrastructure, other species, and many of the most impoverished human beings are unable to do so, creating a very large environmental, economic, and moral problem this century (Patz, 2005).

To avert the more severe scenarios predicted by the IPCC, a great deal of effort is underway to de-carbonize global economies, increase energy efficiency, and conserve energy and natural CO_2 sinks wherever possible. The scope of this challenge is enormous since economic growth has been tightly coupled to CO_2 emissions since the industrial revolution (Garrett, 2011). Furthermore many of the largest global economies (USA,

China, India, Russia, Australia) are endowed with the world's largest coal reserves, a cheap reliable fuel source with the lowest efficiency of combustion for conventional fossil fuels (Schrag, 2009). Like oil, coal consumption has been one of the pillars of industrialization in the developed world. Unlike "peak oil" (Bentley, 2002) where the maximum amount of global oil extraction is reached, we are decades to centuries away from "peak coal"(Mohr and Evans, 2009). Continued exploitation of this resource would push GHG concentrations past targets set by global consortiums such as the IPCC. For 10000 years atmospheric CO_2 concentrations were relatively stable at 280 ± 20 ppm CO_2 (Solomon, 2007); today concentrations are significantly higher at 391.76 ppm (Mauna-Loa-Observatory 2011). To curtail increases in atmospheric CO_2 and maintain or increase the global mean standard of living, multiple technologies will need to be deployed quickly to achieve a stabilization of emissions and ultimate reduction this century (Pacala and Socolow, 2004).

1.2 Proposed Solutions

Increases in atmospheric CO_2 concentrations can be avoided by one of three ways: enhancing and preserving natural sinks, increasing energy efficiency and conservation, and de-carbonizing global energy systems (Pacala and Socolow, 2004). Natural sinks include soils, swamps, and forests; it is estimated that scaling down deforestation efforts in tropical regions to zero by 2050 could prevent 25 Gtons of CO_2 from reaching the atmosphere (Pacala and Socolow, 2004). Energy efficiency can be introduced through vehicle fuel economy, stricter building codes, and proliferation of public transit. Finally de-carbonizing our fuel and energy infrastructure with many existing low carbon technologies would also contribute to significant emissions reductions.

There has been a great deal of needless confusion over what technologies will dominate the 21st century energy sector, which often pits technologies in opposition to one another competing for subsidies and funding (Pacala and Socolow, 2004). Many technologies exist which could stabilize, and ultimately reduce CO_2 emissions, however significant reductions have yet to be realized (Pacala and Socolow, 2004).

Renewable technologies are those that exploit natural transfers of energy on the Earth that are naturally replenished. Examples of these are: solar thermal, solar photovoltaic, on-shore and offshore wind, hydroelectric dams, and biofuels. These technologies are currently burdened by their provincialism. For example solar power is most attractive near the equator, wind power in windy areas, hydro-electric dams on large river systems, and biofuels in areas of high crop yields and a low risk of impacting regional food security or natural carbon sinks. Renewable technologies may dominate global energy infrastructure in the future, however in the transition years away from fossil fuels there can be significant emissions reductions realized through current technologies.

De-carbonizing the current non-renewable energy infrastructure involves many different approaches, some of which target fuel sources. Switching to natural gas-fired power plants from coal-fired power plants greatly increases efficiency since natural gas produces much more energy per unit combusted (Patzek, 2010). Another option is to increase the portion of power produced by nuclear fission reactors. Although nuclear fission reactors have far lower life cycle CO_2 emissions than plants that burn fossil fuels, they take nearly a decade to build, and most cost estimates do not incorporate the potential for catastrophic failure, or the threat of nuclear weapons proliferation. Finally, one proposed idea is to sequester CO_2 emissions captured from large point source

emitters into geologic storage reservoirs, a technology called Carbon Capture and Storage (CCS).

1.3 Carbon Capture and Storage

CCS is a technology that could be applied to any large point source CO_2 emitter such as coal-fired power plants, gas-fired power plants, and fossil fuel processing facilities. CCS is currently in a development stage like many of the above technologies mentioned, where its commercial viability is currently under assessment. Every process involved in CCS, from CO_2 capture, to long term monitoring offers a unique set of challenges, which are the subject of vigorous research programs.

There are three dominant approaches for CO_2 capture being explored and developed in existing projects: post-combustion capture, pre-combustion capture, and oxyfuel combustion (Gibbins and Chalmers, 2008). Post-combustion capture, removes CO_2 from the flue gas (bulk gaseous combustion product) at 50 °C via wet scrubbing with an aqueous amine solution, which is then heated and separated from the CO_2 at 120 °C. Pre-combustion capture involves a two stage combustion process where the fuel first undergoes gasification and partial oxidation, which then allows CO_2 to be removed by dissolving into a solvent between 40-70 bar. Then a synthesis or syn-gas is left over which moves onto a hydrogen gas turbine where power generation occurs. Oxyfuel combustion separates O_2 from air, which is then reacted in the combustion process with recycled CO_2 and H_2O. Each of these CO_2 capture technologies are consistently being improved upon, making it unclear which combination of them will predominantly be used in full-scale CCS projects into the future. Currently, coal-fired power plants are most

economical when incorporating pre-combustion capture, and gas fired power plants are most economical when incorporating post-combustion capture (IEAGHG, 2006).

Once CO_2 is successfully captured from an emissions source it must be transported to its partnered storage site. Transport is not anticipated to be a significant cost factor in the deployment of CCS, however if CCS were made mandatory to all large point source emitters it would require a doubling of existing infrastructure involved in piping fossil fuel (Schrag, 2009). Current estimates per ton of CO_2 transported are approximately 1$ (CAD, 2010) per 200 km (Tore Torpe personal communication IEAGHG summer school 2010).

1.4 CO_2 Storage

Storing injected CO_2 is not the most costly aspect of CCS with cost estimates ranging between 2-10$ (CAD, 2010) per ton of stored CO_2 (Gibbins and Chalmers 2008; Eccles, Pratson et al. 2009), however it is of great concern with respect to emissions accounting, and public safety. There are three potential terrestrial storage reservoirs that have been identified as potential CO_2 storage sites: un-minable coal seams, depleted oil and gas reservoirs, and deep saline aquifers (Yang et al., 2010). Depleted oil and gas reservoirs have the proven ability to store hydrocarbons for millions of years, however they must be developed and isolated in order for CCS to be viable. Un-mineable coal seams are challenging in that it is not well understood whether sufficient quantities of CO_2 can be safely stored in them at economic volumes.

Deep saline aquifers are defined as “porous and permeable media reservoir rocks containing saline fluid” (Michael et al., 2010). They are receiving the greatest amount of attention, because they are comparatively ubiquitous in their distribution, and they have

enormous projected storage capacities (Michael et al., 2006; Yang et al., 2010). This is particularly true for the Western Canadian Sedimentary Basin (WCSB) where the majority of Canadian fossil fuel extraction occurs. Deep saline aquifers have the benefit over other candidate storage reservoirs in that they do not pose immediate conflicts with energy resources.

CO_2 injected into storage reservoirs will exist in a supercritical phase above 31.1 °C and 73.9 bar (Vulakovich and Altunin, 1968) where it exhibits properties of both gas and fluid. Over the lifecycle of injected CO_2, it will be trapped in a combination of four trapping mechanisms: structural, secondary, solubility, and mineral. Structural and secondary trapping involves CO_2 trapped as a free phase in either a large pool beneath a geological structure (structural), or by adsorbing to formation surfaces (secondary). Solubility trapping is the portion of CO_2 that dissolves into the reservoir brine. Mineral trapping is where CO_2 is sequestered through incorporation into a mineral form, for example mineral carbonation reactions involving Mg-silicates (Prigiobbe et al., 2009). The contributions of these mechanisms are dependant upon the reservoir depth, brine chemistry, rock composition, and time. Initially CO_2 will predominantly be in an free phase in a structural trap, then over 10s-1000s of years solubility trapping will consume the majority of CO_2 (Gilfillan et al., 2009).

There are still many aspects of CCS, which need additional research such as: identifying and measuring reaction kinetics of various geochemical processes, developing standard practices for calculating the stability and storage capacities of reservoirs, and identifying where and when geochemical reactions occur within a reservoir over the lifetime of a project. The best way to answer all of these questions is first through

rigorous laboratory and modelling investigations, which measure reaction rates of the CO_2-fluid-rock system along with diffusion coefficients for CO_2 and H_2O and micro to basin scale hydrologic flow regimes. Next this information would be most useful coupled to pilot studies followed by full-scale projects. This would allow for the testing of models, certainty in cost estimates and risk assessments, and create motivation to invest in more complex and accurate predictive modeling tools.

1.5 This work

The two central research objectives of this work are to first evaluate and analyze a proposed CCS project located near Fort Nelson British Columbia, based on criteria established in the literature by Bachu, (2006) and Pokrovsky et al., (2009). Second this work will quantitatively measure the dissolution rates of the Keg River formation in response to CO_2 injection. The first section of this work uses data collected both on-site, and in the laboratory, to geochemically characterize a proposed CO_2 storage reservoir. This involves rock sample characterization through XRD measurements, and fluid measurements by a combination of IC, ICPMS, and spectrophotometric methods. The next portion of this thesis presents experiments with both reservoir rock and fluid collected from the Keg River formation at 105 °C, and 50 bar pCO_2. Experiments exploring reactions at or near reservoir conditions for the purposes of CO_2 storage have only been investigated for the past six years starting with (Pokrovsky et al., 2005). Results for the formation waters are then compared to identical experiments using synthetic brines with the same major ion composition to determine the contribution of trace elements to reaction rates –an area of research that is particularly lacking in the published literature. Following these experiments, the impacts of Sr^{2+} and Zn^{2+} on

dissolution rates of formation rocks with two synthetic brines spiked with the respective ions are investigated.

In summary, this work will evaluate geochemical processes of a potential CCS project in British Columbia, the central objective being to increase the understanding of carbonate reservoir reaction kinetics in the pressure temperature regime of potential carbon storage sites. The confidence that the public bestows on policy makers to properly assess this GHG emissions reduction technology will be based on geochemical simulations, which sufficiently account for the natural complexity of injecting millions of tons of CO_2 into sub surface reservoirs. To ensure both safety and economic viability of CO_2 storage these models and simulations must be based on both standard reservoir information (hydraulic conductivity, porosity, reservoir and caprock fracture pressures) and geochemical data generated from conditions as close to those of natural systems in which they are modeling.

Chapter 2: Carbon Capture and Storage in British Columbia

2.1 Introduction

In an effort to reduce CO_2 emissions, the government of British Columbia and Spectra Energy have partnered to explore the potential of CCS in northeast British Columbia. Spectra Energy currently operates the province's largest point source CO_2 emitter; the Fort Nelson gas plant. This site is an ideal candidate to test CCS at a Mton scale, since gas plants separate CO_2 from the flue gas which is a major cost when applying this technology to other large point source emitters, such as coal fired power plants (Knauss, et al., 2005).

This project is located within the WCSB approximately 20 km to the southwest of Fort Nelson, British Columbia (Figure 2.1). If fully deployed, up to 2 Mtons of CO_2, and potentially H_2S will be injected into the subsurface annually (Crockford and Telmer, 2010). The impact that this amount of GHG reduction would have in the context of British Columbia is shown in figure 2.2 by the red dotted line, which is compared to the current emissions trend on the black dotted line. The Fort Nelson CCS project could reduce the emissions of British Columbia by approximately 3%, annually, over its full-scale operational time period.

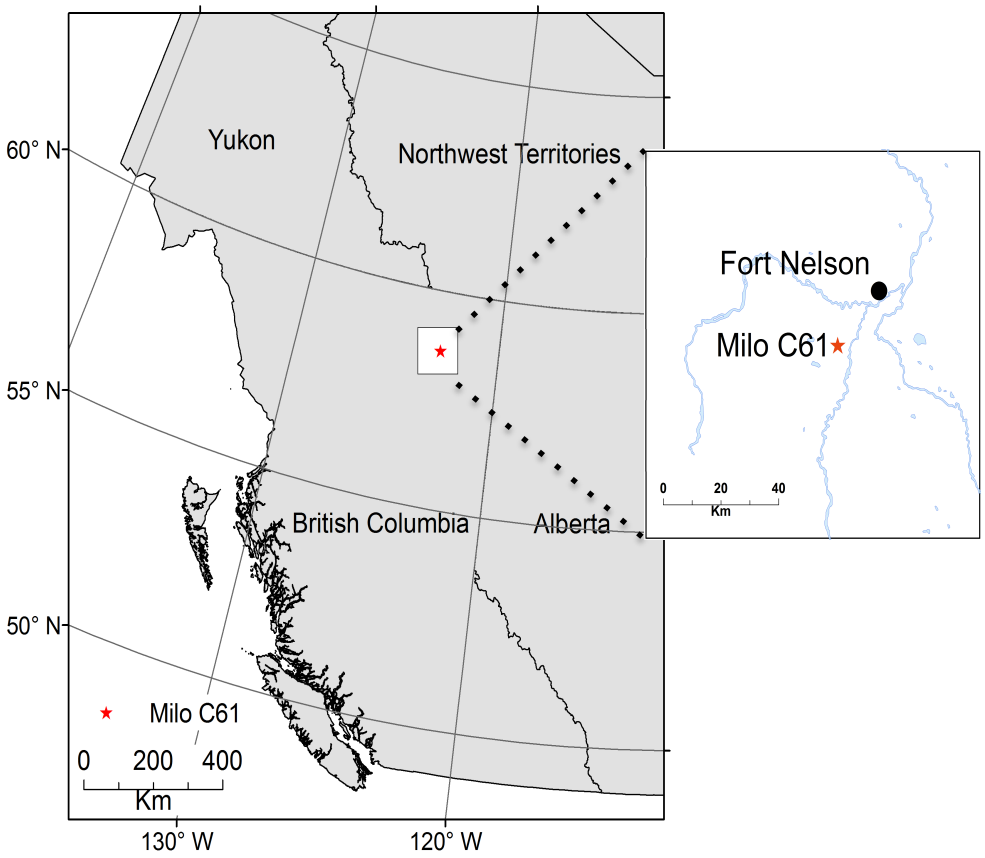

Figure 2.1: A portion of western Canada is displayed, with the location of this study (Milo C61) with a red star, surrounding rivers in blue and the town of Fort Nelson in black.

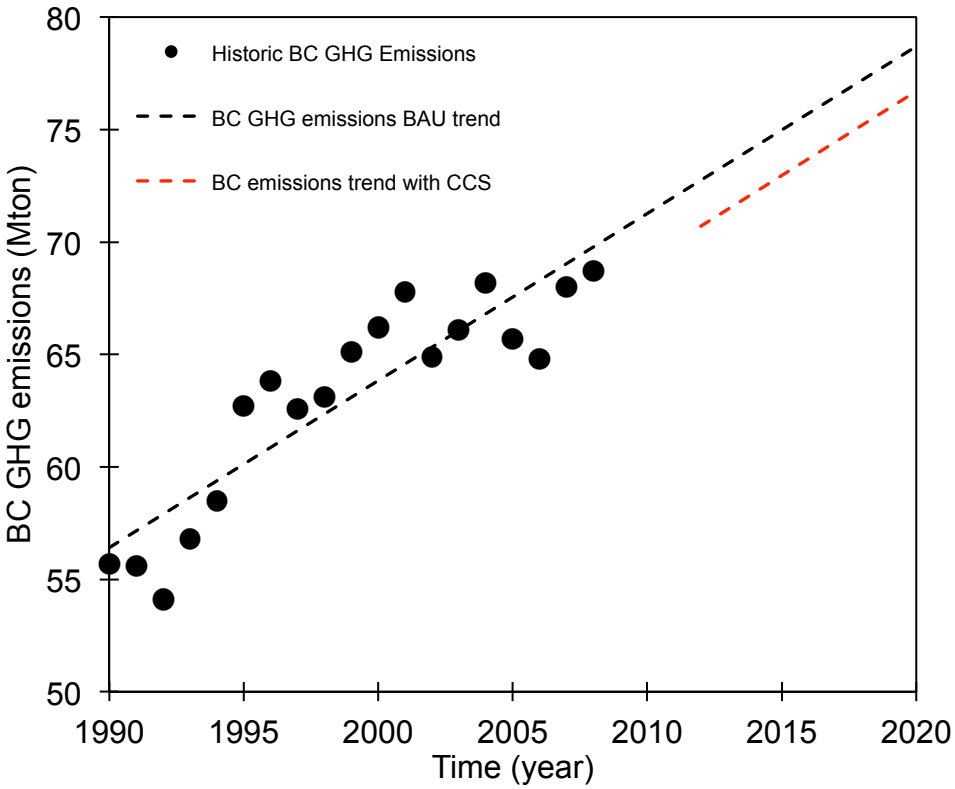

Figure 2.2: GHG emissions of British Columbia 1990-2007 per Mton, compiled by the Greenhouse Gas Division of Environment Canada, the British Columbia Ministry of Forests and the Canadian Forest Service (2008). The current Business As Usual (BAU) emissions trend is displayed in the dotted black line extrapolated to 2020, and the extrapolated (BAU) trend with the proposed Fort Nelson CCS project beginning in 2012 is shown with the red dotted line.

Before the injection of CO_2 into the sub surface can commence, a detailed site characterization study is needed to fully explore the risks, technical challenges, and economic costs a project of this scale could potentially incur. Geochemical information can help to provide answers to some of these questions. This section will evaluate the Fort Nelson project based on a number of geochemical criteria derived from previous studies by Bachu, (2006) and Pokrovsky et al., (2009).

2.2 Geological Background

2.2.1 Regional Geology and Tectonic Setting

The WCSB consists of a wedge of sedimentary material, which is up to 6 km thick in the west beside the Canadian Cordillera, and tapers east toward the Canadian Shield (Al-Aasm, 2003). The WCSB initiated during late Proterozoic rifting of the North American Craton and developed a passive margin succession of mid-Cambrian to mid-Jurassic carbonates with some interlayered shales (Porter, et al., 1982). The geometry of the pre-Cambrian basement structures has exerted strong controls on sedimentation and diagenesis of subsequent sedimentary units (Al-Aasm, 2003). The formation of the Canadian Cordillera has also strongly influenced the tectonic history and sediment deposition within the basin with the greatest influx of material occurring concurrently with the greatest uplift events in the Paleocene and early Eocene (Taylor et al., 1964; Nelson, 1970). The geologic history of the WCSB has made it an active zone for oil and gas exploration, and today it is a highly prospective region for the development of CCS projects.

2.2.2 Stratigraphy

The most prospective CO_2 storage site for the Fort Nelson CCS project is the Keg River Formation, which is a dolomitized carbonate aquifer (Figure 2.3). There are upper and lower portions of the Keg River Formation that are separated through a gradational contact. The protolith rocks that formed the upper Keg River Formation are described as open marine carbonates containing crinoidal columnals and thin-shelled brachiopods (Dunsmore, 1971); the lower section formed through deposition of reefal carbonates

containing stromatoporids and corals (McCamis and Griffith 1967; Dunsmore, 1971). Today the Keg River Formation is laterally extensive sitting below much of northeast British Columbia and northwest Alberta at variable thickness, up to 300 m in some areas and thinnest over the British Columbia – Alberta border. In the Fort Nelson area the Keg River Formation is approximately 200 m thick between 2233.7-2426.0 m depth (Figure 2.3).

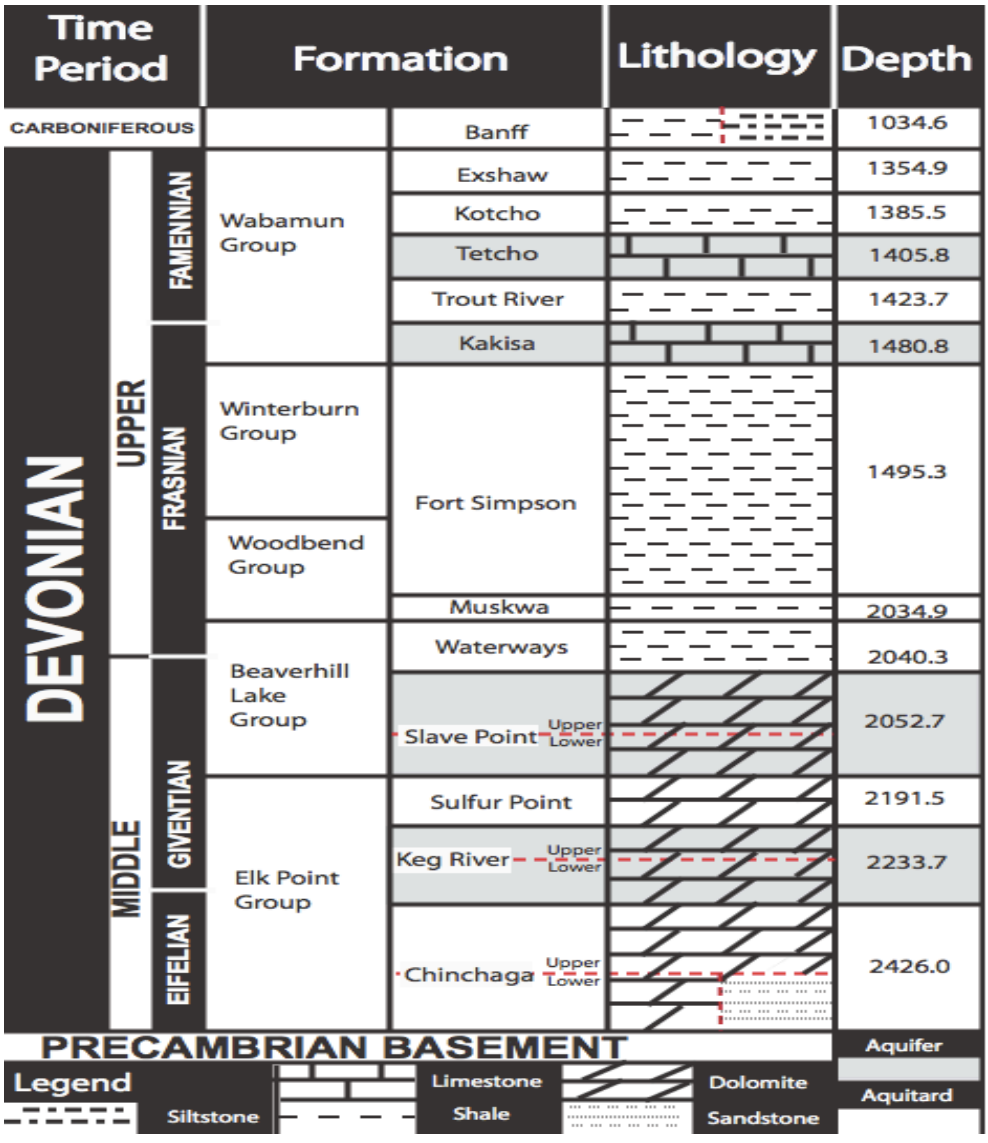

Figure 2.3: Representative stratigraphic column (1034.6m – 2500m) of the Devonian geology of the Fort Nelson area uncovered by Milo C61 drill program May 2009 logged by R. Patterson, (2009).

The Keg River Formation is part of the Elk Point Group, which also includes the Chinchaga Formation below, and the Sulfur Point Formation above (Figure 2.3). The Chinchaga Formation is an aquitard and is above a Precambrian basement, which is an aquiclude. It is also divided into an upper and lower portion with the upper unit meeting the Keg River Formation through a sharp contact. Both upper and lower units of the Chinchaga Formation are predominantly anhydrite with interbedded microcrystalline dolomite with varying quantities of sandstone (McCamis and Griffith, 1967). The top of the Elk point group is the Sulfur Point aquitard, which is composed of carbonates and evaporites (McCamis and Griffith, 1967).

Above the Elk Point Group are the Beaverhill Lake, Woodbend, Winterburn, and Wabamum groups (Figure 2.3). The Beaverhill Lake Group contains the upper and lower portions of the Slave Point Formation, another middle Devonian aged aquifer, and the Waterways Formation, which is a shale aquitard. The Woodbend and Winterburn groups are thick shale aquitards, up to 500 m thick in the case of the Fort Simpson shales; these units would act as thick barriers to any vertically migrating CO_2. At the end of the Devonian sequence in the Fort Nelson area is the Wabamun group, a series of limestone aquifers layered with shale aquitards (McCamis and Griffith, 1967).

The Keg River Formation is the most prospective CO_2 storage location in this package of rock, because it is the deepest aquifer unit allowing larger amounts of CO_2 to be stored in a denser phase and would create the furthest vertical path for CO_2 to migrate in the event of a leak. The Keg River Formation also has high potential porosity 5-20% and permeability 625-16000md measured in the Zama area of northwest Alberta (McCamis and Griffith, 1967).

2.2.3 Dolomitization

Since originally deposited as various forms of calcite, the Keg River Formation has been dolomitized. The origin, timing, and mechanism of this remain unclear and contested (Machel and Lonnee, 2002; Al-Aasm, 2003). A general explanation for this conversion from calcite to dolomite is that high heat-flow in the past as a result of crustal thinning either from extensional margins or early stages of convergent margins (Davies and Smith, 2006), allowed for fluids to flow through extensional faults which permeate through rocks with high primary porosity and permeability (Al-Aasm, 2003). Interaction with rocks containing large quantities of weatherable Mg-bearing minerals such as basalt may have provided a source for the large quantities of Mg incorporated into dolomite. Temperatures of these fluids have been measured between 150-235 °C through fluid inclusions in the Zama area of Alberta (Dunsmore, 1971; Alustead and Spencer, 1985). The timing of this event in the case of the Keg River Formation is unknown but some evidence suggests that it occurred early post Devonian and pre Laramide tectonic event where the Rocky Mountains formed starting in the Cretaceous (Al-Aasm, 2003). Dolomitized reservoirs like the Keg River Formation are highly prospective targets for both CCS, and fossil fuel exploration (Davies and Smith, 2006). The conversion from calcite to dolomite reduces the volume of the rock body allowing for more pore space to open up, which can house fluids such as saline waters.

2.2.4 Fluid Evolution

The waters of the WCSB housed in Devonian carbonates have a distinct aqueous chemistry from brines in laterally equivalent units throughout the basin (Grasby and Chen, 2005). Current data sets have a limited utility for detailed geochemical analysis

needed for a CCS project, however, regional assessments of the basin have made progress in hypothesizing the origin of the fluids housed within Devonian carbonates (Grasby and Chen, 2005). During the time of deposition the Keg River Formation was in the subaqueous environment, with Devonian seawater infiltrating available pore space. This water is thought to have persisted in the basin throughout the remaining Phanerozoic to present day, though geologic events have greatly altered the original aqueous chemistry (Hitchon and Friedman, 1969; Aulstead and Spencer, 1985).

One of the earlier events in the brine evolution is subaerial evaporation that concentrated the paleo-seawater (Aulstead and Spencer, 1985; Connolly et al., 1990). Next this water is thought to have sunk into deeper geologic units where it was heated and interacted with deeper rocks (Aulstead and Spencer, 1985), which may have been what caused dolomitization (Davies and Smith, 2006). Since these events waters have been diluted, which is expressed through low salinity values of 20-320 g/L (Grasby and Chen, 2005). It is thought that meteoric water is the cause of this dilution specifically through thick Pleistocene ice sheets, which reversed basin flow from the post and pre glacial flow regime where waters flow from deeper sediments in the southwest to shallower sediments in the northeast (Hartling, 2008) (Figure 2.4), forcing fresh subglacial surface waters to mix with deep basin waters (Connolly et al., 1990). Evidence of this phenomenon is seen through direct analogues in northern Europe (Boulton et al., 1996), and stable isotope data (Grasby and Chen, 2005).

ion operations. mentary Basin. The flow is topographically driven from a

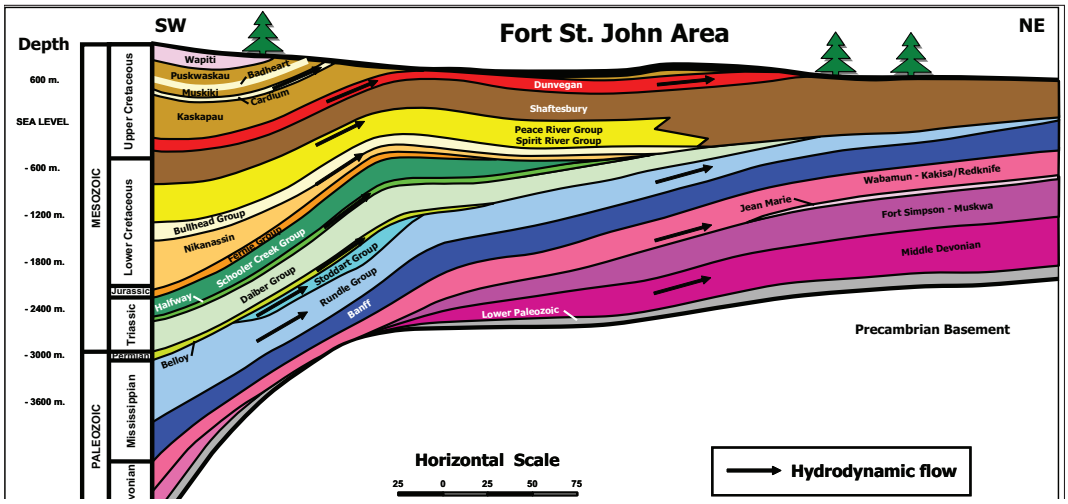

Figure 2.4: This figure from Hartling, (2008) depicts hydroynamic flow of the Fort St. John area, which is located approximately 300 km south of and is directly comparable to the Fort Nelson area. This figure shows that fluid flow is generally from the southwest to northeast.

Other processes that have contributed to the evolution of the brine chemistry in the Devonian carbonate systems of the WCSB are membrane filtration, and interactions with clays (Billings et al., 1969). Understanding the role that past geologic events can have in creating a strong CO_2 storage candidate can help to identify future storage reservoirs of similar origins.

2.3 Methods

2.3.1 Sample Collection

In May 2009, samples of both rock and fluid were collected at Spectra Energy's Milo C61 drill site (Figure 2.1). Solids used in this work were collected as approximately 10 g aliquots of rock cuttings, every 5 m drilled, over the 2500 m hole. Samples were matched to specific depths in the drill hole using tracers placed into the drilling fluid circulation routine. Cuttings sizes varied throughout the entire hole. Most samples ranged between pebble and fine sand sized grains, raising a potential source of error in depth matching, as finer size fractions will remain entrained in the drilling fluid for longer

durations than larger ones. Once extracted rock chips were rinsed “repeatedly with distilled water and dried at 30 °C over night” (R. Patterson, -well-site geologist- pers. comm.).

Fluid samples were collected during drill stem tests, in which the targets (Keg River, Sulfur Point, Slave Point) were isolated with packers and then water was drawn up the drill column and brought to the surface for sampling. In total 20 samples were collected from wet drill pipe, by first pouring into 20 L buckets, and then transferring into 1 L bottles. The bottles were rinsed three times with distilled water, compressed to remove headspace, and sealed with caps and electrical tape.

2.3.2 On-site Solution Measurements

Immediately after water samples were collected, preliminary analysis was conducted to measure temperature, and pH. Measurements of pH utilized both pH indicator strips and an IQ120 minilab pH meter, calibrated with three NIST certified Oakton® buffers (pH = 4.01, 7.0, and 10.0) with an accuracy of ±0.01 pH units, and auto-corrected for temperature. Temperature was measured using a digital thermometer with an accuracy of ±0.1°C.

After sampling, additional water analysis took place, including tests for hardness [Ca^{2+}, Mg^{2+}], chlorinity [Cl^-], and alkalinity [HCO_3^-]. All measurements were made by titrations: alkalinity using phenolphthalein and bromocresol green indicators and H_2SO4 titrant; hardness, using Erio-T indicator and ethylenediaminetetraacetic acid titrant; and chlorinity, using K_2CrO_4 indicator and $AgNO_3$ titrant. Gas content of the fluids brought to the surface was not measured, however, during the extraction of drill pipe from the

Sulphur Point Formation, up to 89 ppm H_2S was detected, indicating that some sour gas resides within the target formations.

2.3.3 Formation Conditions

Formation conditions were measured within the drill hole using a suite of Schlumberger® tool assemblies to measure density and resistivity at various depths. A modular formation dynamics tester was used to obtain the formation pressure and temperature conditions, which determined parameters for experiments discussed later in this thesis.

2.3.4 Solid Analysis

Off-site solid analysis of the Keg River Formation was conducted at the University of Victoria and University of British Columbia and included mineralogical and morphological analysis, of drill cuttings. Mineralogy was determined by X-ray diffraction Rietveld analysis (XRD) (Rietveld, 1966), conducted at the University of British Columbia, in Vancouver, Canada. Samples used in this analysis are prepared by first grinding up in a ring mill, and then sieved through a No. 200 mesh, which isolates the sub 75 μm fraction. Crushed cuttings were divided into two fractions representing the upper and lower portions of the Keg River Formation. This involved homogenizing samples collected at different depths. Samples were then placed under ethanol in a vibratory McCrone® Microrinsing Mill for 7 min. Data was collected using CoKa radiation with a Bruker D8 Focus Bragg-Brentano diffractometer equipped with LynxEye detector, an Fe monochromator foil, diffracted-beam Soller slits and a 0.6 mm (0.3°) divergence slit over a range of 3-80°2θ, operated at 35 kV and 40 mA with a take-off angle of 6.0°. The

International Center for Diffraction Database PDF-4 was combined with Siemens® Search-Match software and Bruker® AXS Rietveld Topas 4.2 to give quantitative phase distributions of minerals in samples.

Surface morphology of individual grains was examined by secondary electrons with a Hitachi® S-4800 field emission scanning electron microscope with an electron beam set at 1 kV at the University of Victoria.

2.3.5 Fluid Analysis

Water samples were prepared for anion and cation analysis first by filtering through a 0.200 μm membrane, next by diluting samples 100 times with deioniozed MilliQ® (18.2 MΩ) water, and finally by acidifying the cation fraction to 0.2% HNO_3. Samples were stored during the interim at 2 °C in a dark storage facility.

Water analysis was conducted using a Dionex® DX-600 ion chromatograph (IC) and a Thermo® XSll X7 quadrupole inductively coupled plasma mass spectrometer (ICPMS) for major cation analysis, and ICPMS for minor cation measurements. The IC was run using an injection volume of 25 μL and an integration time of 15 min. Replicate analysis of standard reference material SLRS-4 (Ottawa River water) determined the accuracy and precision on both instruments, which varied dependent upon the analyte. To account for drift between analyses and matrix corrections when using the ICPMS, samples were spiked with Rh, In, Re, and Bi to use as internal standards.

Additional analysis was conducted to measure HCO_3^-, S, and Cl-. The concentration of HCO_3^- in solution was determined using a Hach digital titration kit with bromocresol green methyl red color indicator and 0.16 N H_2SO_4 titrant added in 1.25 μL

aliquots accurate to ±1.0%. Sulphur species were measured by spectrophotometric adsorption at 610 nm wavelength in a 10 cm cell and calculated using Beer's law, (Eqn 2-1) which relates the absorbance of light A, the molar absorbitivity e ($L \cdot mol^{-1} \cdot cm^{-1}$), the path length of the sample *b* (cm^{-1}), and the concentration of the analyte *c* (SO_4^{2-}) ($mol \cdot L^{-1}$). Although SO_4^{2-} was the species measured, it is unlikely that sulphur exists in the reservoir in this form due to the presence of pyrite, and minor amounts of H_2S in overlying formations during drilling. Samples were calibrated with five in-house standards: 0, 1, 2, 5, and 10 ppm SO_4^{2-}. Chlorinity was measured via titration with K_2CrO_4 indicator and $AgNO_3$ titrant.

(2-1) $A = ebc$

2.3.6 Equilibrium modelling

The Geochemist's Workbench® (GWB) version 7.0 was used to evaluate whether the aqueous system in the Keg River Formation is in geochemical equilibrium with the mineral phases present. The program Spece8 was used for equilibrium calculations with the database Thermo.dat, constructed at Lawrence Livermore National Laboratory. Multiple simulations were conducted at variable Ca^{2+} and Mg^{2+} concentrations to determine the contribution of the different ionic species.

2.4 Results

2.4.1 Formation Fluid Determination

In order to separate true Keg River brine from the drilling fluid, pH and total hardness were monitored. Drilling mud pumped into the hole is basic, with a pH of approximately 11; in contrast the formation brine is more acidic with pH values between 6 and 7. The transition between these two fluids was visually observed with initial fluids

brought up to the surface having a strong drill fluid signature with a milky brown colour. This was followed by a sharp transition region, and finally, true Keg River brine which was a dark brackish colour (Figure 2.5). Total hardness (Ca, Mg) values also depict this transition with drill fluid having a much lower hardness than Keg River brine (Figure 2.5). Waters with low pH, and high hardness values were assumed to be true Keg River brine and were used for further analysis and experiments.

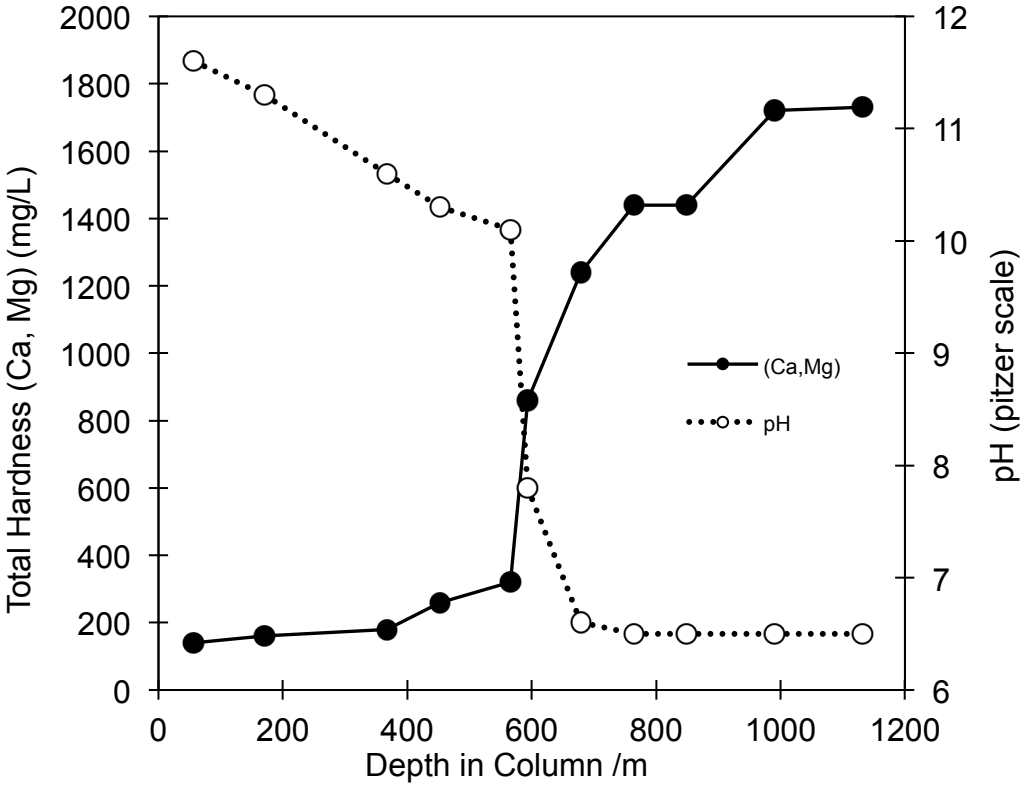

Figure 2.5: Determination of Keg River brine through measurements of total hardness and pH performed at Milo C61 drill site. Each point equals an average of three measurements with standard deviations within the size of the data points. Water samples used in subsequent work were selected from waters of pH values of approximately 6.5 and a total hardness of >1600 mg/L.

2.4.2 Formation Conditions

Results from on site measurements indicate that the Keg River Formation exists at a pressure of 194 +/- 0.007 bar and a temperature of 105 +/- 0.5 °C (Table 2.1). Under these conditions the Keg River Formation is characterized as a relatively warm

environment with an elevated geothermal gradient (Bachu and Burwash, 1994). Uncertainty in the depth of the Keg River Formation, which temperatures and pressures were measured, is because during the drill stem test the lower packer lost its seal, thus only constraining the top packer depth.

Table 2.1: Formation information and measurements taken on site from MiloC61 Drill site in May 2009.

Parameter	Value	Analysis Location
Formation	Keg River	N/A
Depth (m)	2280	Down hole
Pressure (Bar)	194 +/- 0.007	Down hole
Temperature (°C)	105 +/- 0.5	Down hole
pH	6.5	Surface, on site
$[HCO_3^-]$ (meq/L)	14.4	Surface, on site
Total Hardness (ppm)	1720	Surface, on site
Chlorinity (ppm)	12300	Surface, on site

2.4.3 Solid Analysis Results

XRD analysis shows that the Keg River Formation consists of predominantly dolomite and calcite with minor amounts of quartz and trace amounts of pyrite, and muscovite (Table 2.2) (Appendix I). Comparisons of upper and lower Keg River mineralogy show a decrease in the amount of dolomite and an increase in the amount of calcite with depth (Table 2.2). There are also decreases in both quartz and pyrite from upper to lower Keg River samples, and the appearance of muscovite in the latter.

Table 2.2: XRD, Rietveld refinement analysis conducted at the University of British Columbia

Mineral (wt%)	Upper Keg River	Lower Keg River
	Depth(m): 2235 – 2365	2365 - 2420
Dolomite	92.97	86.28
Calcite	5.08	8.87
Quartz	1.81	3.62
Pyrite	0.14	0.50
Muscovite	0	0.73

2.4.4 Fluid Chemistry Analysis

Keg River brine is predominantly composed of Na^+ and Cl^-, with significant Ca^{2+}, K^+, Mg^{2+}, HCO_3^-, and S. The Keg River brine has a Ca:Mg ratio of approximately 5:1. Significant minor element contributions to brine chemistry include Li^+, Sr^{2+}, Zn^{2+}, Al^{3+}, Fe^{2+}, and Si^{2+}. Minor inconsistencies occurred between IC and ICPMS data when comparing measurements for the same waters, however there was only a 3% variation between both methods, giving high confidence in the results.

Results from calculations using Spec8 GWB V.7.0, suggest that at current concentrations of Mg^{2+}, and Ca^{2+} (Table 2.3) (Figure 2.6) the saturation index of the Keg River Formation is between approximately 1.0 and 2.5 dependent upon the mineral. Equilibrium was calculated with respect to these mineral saturations because dolomite represents approximately 87-93% and calcite approximately 5-9% of the Keg River Formation mineral assemblage (Table 2.2). Injecting large volumes of CO_2 will undoubtedly introduce some dramatic geochemical shifts in the formation fluid. These potential changes are explored further in Chapter 3 of this thesis.

Table 2.3: Fluid analysis of Keg River formation brine by IC, ICPMS, titrations, and spectrophotometry compared to both SMOW and riverine waters presented by Li et al., (1982).

Ion	Value (mmol)	Method	Riverine (mmol)	Seawater (mmol)
Cl^-	271	Titration	0.220	530.280
Na^+	211	IC	0.274	469.776
HCO_3^-	24.6	Digital Titration	0.261	0.459
Ca^{2+}	23.5	IC	3.743	10.480
K^+	15	IC	0.059	9.719
SO_4^{2-}	5.2	Spectrophotometry	0.039	9.421
Mg^{2+}	5.06	IC	0.169	53.075
Si^{2+}	7.19	ICPMS	0.231	0.071
Li^+	2.32	IC	4.32E-04	2.88E-04
Sr^{2+}	1.04	ICPMS	7.99E-04	9.13E-02
Fe	0.48	ICPMS	7.16E-04	3.58E-05
Zn^{2+}	0.2	ICPMS	3.06E-04	4.59E-06
Al^{3+}	0.13	ICPMS	1.85E-03	3.71E-05
Ba^{2+}	0.0395	ICPMS	1.46E-04	1.46E-04
Rb^+	0.029	ICPMS	1.17E-05	1.40E-03
Mn^{2+}	0.0138	ICPMS	1.27E-04	7.28E-07
Pb^{2+}	9.13E-4	ICPMS	4.83E-06	9.65E-09
Mo^{2+}	8.33E-4	ICPMS	6.25E-06	1.04E-04

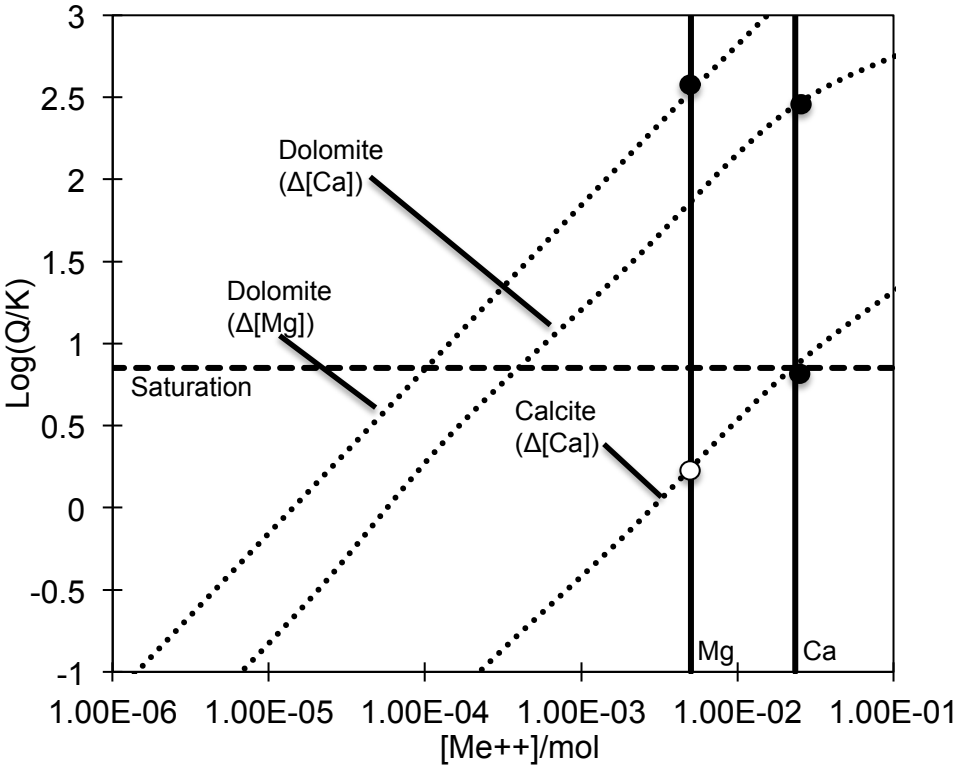

Figure 2.6: The degree of both dolomite and calcite saturation (diagonal trending dotted lines) as consequences of changing Mg, and Ca concentrations in a system replicating Keg River brines (Table 2.1 and 2.3). Concentrations of Mg and Ca present within the Keg River system are solid vertical lines. The reservoir ion concentrations show both dolomite and calcite are in a state of supersaturation. Because calcite is not readily precipitating in the reservoir, the saturation of dolomite has been normalized to calculated calcite saturation. Dolomite is not readily precipitating in the reservoir because of the high activation energy of formation (Morse and Arvidson, 2002). Results were calculated on the Geochemists Workbench V.7.0.

2.5 Discussion

2.5.1 Formation Conditions

The pressure and temperature conditions of a CO_2 storage reservoir are important factors to consider when attempting to quantify the amount of CO_2 that can be stored underground. CO_2 is a compressible gas, and under the pressure and temperature conditions (194 +/- 0.007 bar; 105 +/- 0.5 °C) measured in this work, injected CO_2 will have a density of approximately 490 $kg \cdot m^{-3}$ (Vukalovich and Altunin, 1968). This means CO_2 will occupy over two times the volume of the water it replaces by mass upon

injection. Therefore the greatest pressures experienced within a reservoir will be during the injection period, which will consequently be the period of greatest risk (Mathias et al., 2009). The high temperatures experienced in the Keg River Formation will also impact the viscosity of CO_2 injected, with higher temperatures reducing the viscosity (Vukalovich and Altunin, 1968). This is amenable to CO_2 injection because increased volumes of CO_2 can be injected at greater rates without a build up of critical pressure that could potentially compromise the ability of the reservoir to safely store CO_2 (Mathias et al., 2009).

Over geologic timescales solubility trapping will consume the majority of CO_2 compared to other mechanisms such as mineral, and structural trapping (Gilfillan et al., 2009). Pressure and temperature conditions also affect the amounts of CO_2 that will dissolve into the brine. At the pressure and temperature conditions experienced in the Keg River Formation the solubility of CO_2 in the brine will be between 0.9 and 1.2 $mol \cdot kg^{-1}$ (Duan and Sun, 2003). Relatively high pressures in the formations such as those found in the Keg River (194 +/- 0.007 bar) will increase CO_2 solubility, however the temperature of 105 +/- 0.5 °C exists in a CO_2 solubility low, where the least amount of CO_2 will dissolve into the brine, near 100 °C (Duan and Sun, 2003).

2.5.2 Formation Rock

The mineralogy presented in this work (Table 2.2) is consistent with previous studies of the Keg River Formation (Griffin 1967; McCamis and Griffith 1967; Dunsmore 1971; Aulstead and Spencer 1985). The geology of the Fort Nelson area is attractive for CCS, because Mg-bearing carbonates, in this case dolomite, are much less reactive than their progenitor, calcite (Plummer, Wigley et al. 1978; Pokrovsky, Schott et al. 1999).

The high geothermal gradient in the Fort Nelson area (Table 2.1) also reduces the solubility of both dolomite and calcite (Ellis, 1959). This is important since large amounts of dissolution particularly around the injection center, may lead to formation instability and sediment compaction, which could potentially compromise caprock integrity (Liteanu and Spiers, 2009).

Injectivity is important in CCS projects particularly when coupled to the volume of CO_2 to be injected. It controls the number of wells that must be drilled to deliver CO_2 to the storage reservoir. Work presented here was not able to determine the parameters controlling injectivity (porosity and permeability) of the formation as samples were collected as drill chips. A reasonable estimate however, can be deduced from the geometric mean of previous studies on the Keg River Formation in the Zama area of Alberta with a porosity and a permeability of approximately 12.5% and 8300 md respectively. Even upon the discovery of this information, both natural and induced fracture permeability will likely dominate fluid migration pathways, and this is difficult to extrapolate from a single drill core and at this stage of storage site evaluation.

2.5.3 Formation Fluids

The chemical composition of the Keg River Formation fluids determined in this work is in agreement with previous studies that interpreted the brine chemistry to be a result of paleo seawater experiencing subaerial evaporation, membrane filtration, interaction with deeper formations, and finally being diluted by meteoric water brought on through the Pleistocene glaciations (Billings et al., 1969; Hitchon and Friedman, 1969; Aulstead and Spencer, 1985; Connolly et al., 1990; Grasby and Chen, 2005). Similarity of ratios with major elements between the Keg River Formation and Standard Mean

Ocean Water (SMOW) (Figure 2.7) (Table 2.4) is evidence that waters currently within the Keg River Formation originated as paleo seawater.

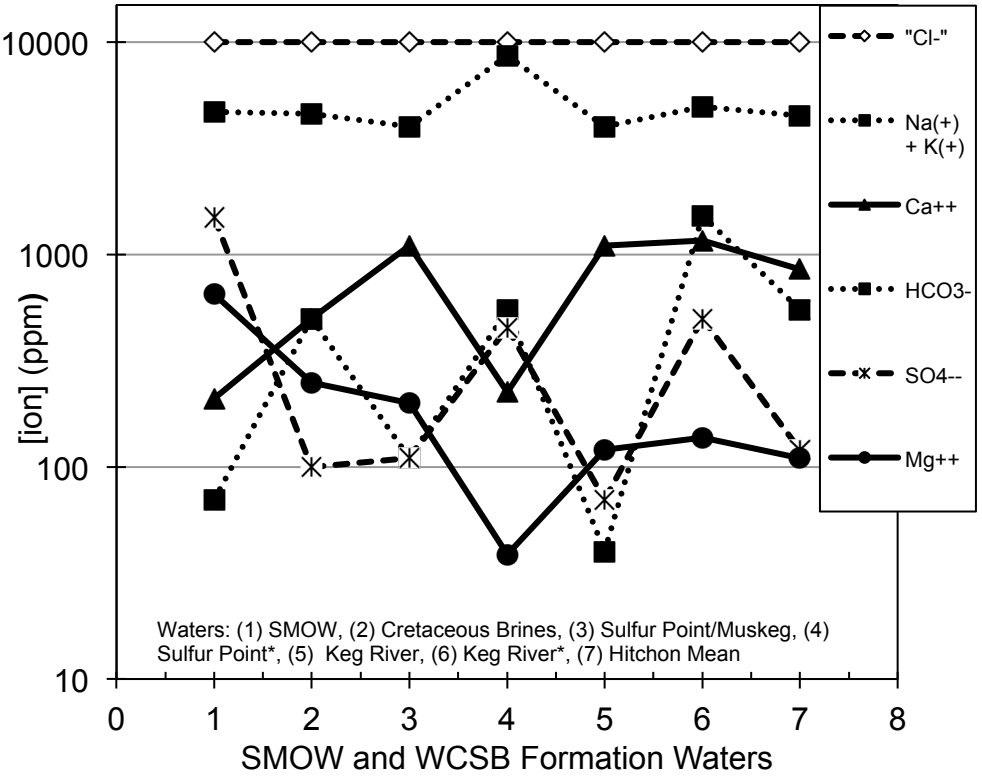

Figure 2.7: Comparison of Keg River formation water to overlying strata sampled in this study, and by Dunsmore, (1971), and Hitchon (1969). These values are normalized to [Cl-] = 10000 ppm and compared to SMOW. This figure has been adapted from Dunsmore, (1971). *Indicate waters from this study. Errors bars on values presented are within the size of the data points.

Table 2.4: Comparison of waters of this work with SMOW, and Hitchon mean ocean water (Hitchon et al., 1969)

Waters	$[Cl^-]$ (mmol)	K/Na (by wt.)	K/Li (by wt.)
Seawater	545	0.036	2280
Hitchon et al., 1969	758	0.039	52.4
This work	271	0.121	36.3

When a body of seawater evaporates, halite will be the first mineral to precipitate out, which will remove equal portions of Na^+ and Cl^- from solution, but retain elevated concentrations of other ions in solution. Evidence of this is seen through the relatively high ratio of K^+ to Na^+(Table 2.4) in Keg River waters.

Ion ratios can also be useful in determining the amount of membrane filtration, which is when large ions are selectively retained in solution over smaller ions when forced through rocks with very small pore spaces (Billings et al., 1969; Hitchon et al., 1971). Fluid analysis in this work found a deviation in the ratio of K^+ to Li^+ with increased amounts of K^+ (Table 2.4); this was interpreted as signifying the occurrence of membrane filtration at some point in the fluids history.

When present day levels of ions in solution in the Fort Nelson area Keg River Formation are compared to SMOW, it is found to be relatively fresh, in fact it is more dilute than waters housed in the Keg River Formation in other parts of the WCSB (Table 2.4) (Billings et al., 1969; Dunsmore, 1971). If consistent with work conducted in other parts of the WCSB than this dilution occurred during the Pleistocene glaciations, which is supported through isotopic analysis of waters and a basin-wide hydrodynamic flow model (Connolly et al., 1990; Grasby and Chen, 2005).

Although the Keg River Formation throughout the WCSB has experience many of the same significant geological events there is a diversity of brine chemistry throughout the formation. This is made more apparent when values of previous studies (Hitchon et al., 1969; Dunsmore et al., 1971) are normalized to Cl^- concentrations and plotted against one another (Figure 2.7). In the Fort Nelson area fluids contain comparatively high levels of S and HCO_3^- but very similar relative concentrations of Na^+, Mg^{2+}, and Ca^{2+} (Figure 2.7). These differences likely reflect the diversity in the timings and interactions waters in the Keg River Formation throughout the WCSB have experienced since original deposition. More significantly, other findings found from analysis of Fort Nelson area waters is that the overlying Sulphur Point Formation has distinct brine chemistry from the

Keg River Formation (Figure 2.7). Differences are most apparent through the relatively low concentrations of Mg^{2+} and Ca^{2+}, but high concentrations of Na^{+}, HCO_3^{-} and S.

Natural fluids found in deep formations have a complex chemical composition, giving insight into their past. This information is useful in evaluating the brine as a potential CO_2 storage reservoir. The brines studied in the Keg River Formation were found to be relatively fresh, which increases the capacity of the brine to accept CO_2 (Duan and Sun 2003), which will be the dominant trapping mechanism over millennial timescales (Gilfillan et al., 2009). Another important insight is that Keg River brine is distinct from overlying fluids in the Sulphur Point Formation, suggesting that the Keg River Formation is sealed from overlying strata, avoiding the risk of CO_2 leakage. The composition of these fluids will also impact how the solids of the reservoir respond to CO_2 injection, a topic covered in Chapter 3 of this thesis.

2.5.4 Geochemical Predictions

Upon injection CO_2 will readily dissolve into the brine where reactions with water yield HCO_3^{-} and H^{+}. This decreases the pH of the solution from a pH of 6.5 to a more acidic regime near a pH of 5 (Pokrovsky et al., 2009). Modeling results depict a geochemical regime where dolomite is supersaturated in solution, indicating that the system exists in pseudo equilibrium, where minerals are not precipitating or dissolving into the brine (Figure 2.6). The drop in pH when CO_2 is injected will be buffered to a degree through heterogeneous reactions that may involve the dissolution of formation rock, both reducing rock volume, and stabilizing pH values. The degree to which this occurs is important in estimating changes in porosity and permeability of the formation, however the rate this occurs is partially dependent on the original permeability and

porosity of the rocks that the acidified brine interacts with. Quantifying both the rate constants and degree to which the formation rocks dissolve must be investigated for a more comprehensive understanding of the response of the subsurface to CO_2 injection.

2.5.5 Co-injection of H_2S

An important issue not investigated in this work, are the impacts co-injected H_2S with CO_2 will have on the Keg River Formation. Hydrocarbons containing H_2S are common throughout the WCSB. As of 2003 over 2 Mtons of H_2S was injected into the sub-surface for enhanced oil recovery purposes (Bachu and Gunter, 2005), and today there are 40 acid gas injection wells in Alberta alone (Hawthorne et al., 2010). Co-injecting impurities is attractive because purifying CO_2 streams can consume up to 75% of the total cost of CCS (Knauss et al., 2005), and because it reduces the cost of handling and transporting the large amounts of S produced in gas refining. For these reasons it is important to consider the geochemical impacts of co-injecting H_2S with CO_2. Currently there are few experimental studies involving H_2S due to the associated risks and hazards, therefore the majority of previous work has focused on geochemical modelling.

Previous studies using geochemical modeling tools, have found that upon co-injecting CO_2 and H_2S into a reservoir, H_2S will diffuse more rapidly to the edge of the CO_2 plume (Ghaderi et al., 2011; Shevalier et al., 2011). The behaviour of the H_2S phase is dependant upon the gas saturation of the brine, with H_2S partitioning into the brine preferentially over CO_2 (Ghaderi et al., 2011). Of the experimental studies that do include H_2S, the reactivity of minerals in contact with either CO_2 or CO_2-H_2S systems has not varied significantly (Shevalier et al., 2011). In both cases dissolving CO_2 will acidify formation waters even after the formation rocks buffer aqueous reactions. The reaction

products of H_2S containing gas, however, have been reported to differ from that of pure CO_2 injection (Holubnyak et al., 2011).

The Fort Nelson Project has the potential for up to 80% H_2S to be co-injected with CO_2 per year (Dave Moffat, Spectra Energy Personal Communication). Although H_2S was not detected during drilling of the Keg River Formation this does not preclude the possibility that minor amounts may exist in the formation. In fact upon the extraction of waters from the overlying Sulphur Point Formation (Figure 2.3) minor amounts of H_2S were released. The source of the H_2S may be due to thermochemical sulphate reduction where heated evaporates release H_2S (Machel et al., 1995; Shevalier et al., 2011). This would be consistent with the high geothermal gradient in the area, and known contact with hydrothermal fluids in the past (Dunsmore, 1971). Ongoing modelling, laboratory and field investigations will help to articulate the specific contributions that H_2S makes in CCS projects.

2.5.6 The Keg River Formation as a CO_2 Storage Site

The Fort Nelson Project has high potential as a CO_2 storage project from an economical standpoint, because CO_2 is already separated from sour gas processed at the refinery, and the province of British Columbia has provided an incentive to storing emissions through a carbon tax. The Fort Nelson Gas Plant is also a large point source emitter located far away from any major population center, and it exists in an area of active gas development, which provide the existing experience and infrastructure needed. It is also relatively attractive from a political standpoint in that it exists in a country that has large basins with enormous storage potential, and a majority population, which accepts the scientific consensus of anthropogenic global warming.

Technical criteria that have been established in previous work has also been met for this project. The Keg River Formation is located in a tectonically stable area, and exists at a depth below the Fort Nelson area where CO_2 would exist in a dense supercritical state minimizing storage volume (Bachu, 2008). The overlying rock strata of evaporites, and shale would act as effective hydrodynamic barriers to CO_2 leakage. Further information is needed however to fully assess this reservoir including the potential for interference with hydrocarbon development, local and regional hydraulic conductivity, and the fracture pressure of both the reservoir rock and caprock (Shukla et al., 2010).

Geochemical aspects of this project are also within recommendations made by Pokrovsky et al. (2009), in that the Keg River Formation consists of predominantly dolomite with minor amounts of calcite (Table 2.2). The dolomite will be less reactive maintaining reservoir stability while the calcite will provide an input of HCO_3^- to buffer the pH of solutions keeping them less reactive (Pokrovsky et al. 2009). The physical conditions are also amenable to CCS with temperatures between 100-150 °C and pCO_2 values greater than 50 bar which will also reduce mineral dissolution moving the system closer to saturation (Pokrovsky et al., 2009).

2.6 Summary

The Keg River Formation is located at a depth of approximately 2200 m, where pressure and temperature conditions are 194 +/- 0.007 bar, and 105 +/- 0.5 °C. Measurements of fluids sampled, describe a predominantly Cl^-, Na^+, HCO_3^-, Ca^{2+}, K^+, Si^{2+}, S and Mg^{2+} brine with trace amounts of Mn^{2+}, Zn^{2+}, Li^+, Sr^{2+}, and Ba^{2+}. Solid

analysis identifies that these waters are contained within middle Devonian carbonates, composed of dolomite and calcite with minor quantities of quartz, pyrite, and muscovite.

Analysis show that the Keg River Formation waters are distinct from those of the overlying Sulphur Point Formation, suggesting that no exchange is occurring between these units. Furthermore, waters sampled from the Keg River in the Fort Nelson area are relatively fresher than waters from the same formation sampled in Alberta. This is conducive to storing more CO_2 within the aquifer brine because more CO_2 can dissolve into waters of lower ionic strength (Duan, 2003). This suggests that the Keg River Formation is a strong candidate to test the viability of CO_2 storage in the subsurface of the Fort Nelson area.

2.7 Future work

Characterization of Keg River Formation fluid in this study did not measure the full suite of anions in solution. This analysis could be performed on an IC instrument, and would provide a full characterization of fluids within the formation. This contribution would likely be relatively small in the effects of CO_2 injection into a reservoir since the major anions in solution Cl^- and HCO_3^- were measured (Ruiz-agudo et al., 2010).

Similarly further chemical analysis of specific minerals would allow geochemical modeling of trace elements incorporated into the matrix and their exchange reactions with the aqueous phase (Lumsden, and Lloyd, 2008). This approach would also allow for the determination of the ratio of Ca and Mg, which would have some influence on the interpretation of dissolution rate data. These analyses could be performed using laser ablation coupled to ICPMS, and running transects along mineral surfaces. This

knowledge would allow a more complete understanding of saturation states of natural formation rock with complex surface reactions involving trace elements, and better predictions pertaining to the injection of CO_2 into the system (Lumsden, and Lloyd, 2008).

Finally this work could be expanded upon by having access to more study sites, with the knowledge that the subsurface is heterogeneous and one drill core cannot encompass the full complexity of a carbonate reservoir. More samples of the Keg River Formation in the Fort Nelson area along with natural and synthetic end members, would allow the construction of a more comprehensive picture of this potential CO_2 storage reservoir.

Chapter 3: Dissolution kinetics of the Keg River formation in real and synthetic brines

3.1 Introduction

Carbonate minerals house approximately 60% of global oil reserves (Morse and Mackenzie, 1990), and may become the locations of many CO_2 storage sites. Insights into the formation and composition of carbonates on a thermodynamic basis has been well explored (Ellis, 1959; Szramek et al., 2007). It is becoming clear however that reaction kinetics of carbonates also play an important role in regulating not only formation water compositions, but also the capacity of reservoirs to house CO_2 (Ganor and Lasaga, 1998). Upon injection, CO_2 will form a plume at the top of the reservoir and migrate laterally. At the CO_2-aquifer-fluid interface a mixed fluid region will form over time where the geochemistry of the original aquifer fluid will be dramatically altered (Figure 3.1). Quantification of reaction rates in this region is critical to accurately predict the impact injected CO_2 will have on a storage reservoir.

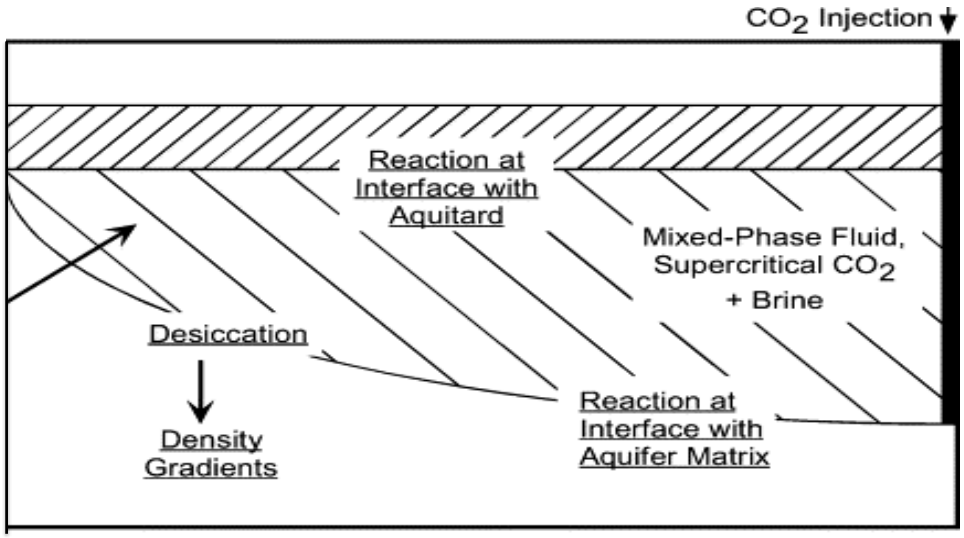

Figure 3.1: This figure is adapted from Kaszuba et al., (2003), where it is shown that injected CO_2 will create a mixed fluid phase where the most dramatic geochemical changes will occur in a storage operation.

With CCS under consideration as a pillar of CO_2 reduction strategies, a growing number of studies are exploring the potential of carbonate reservoirs to store CO_2. Kinetics studies on the dissolution of carbonates have predominantly focused on calcite with applications to chemical oceanography at temperatures between 0-30 °C, and pressure conditions at or near 1 bar (Sjoberg and Rickard, 1984; Gledhill and Morse, 2006). Results from these experiments are not directly applicable to CO_2 storage projects, which often involve dolomitized reservoirs at much greater pressure and temperature conditions.

Kinetic studies on the dissolution of carbonate rocks at potential reservoir conditions are increasing (Pokrovsky et al., 2005; Gautelier et al., 2007; Pokrovsky et al., 2009), however there are thermodynamic data gaps in databases covering the full array of pressure, temperature, pCO_2, salinity, and fluid and rock compositions that may be encountered in natural storage operations.

3.1.1 Rate Equations for the Dissolution of Dolomite

Previous work on the dissolution of carbonate minerals has led to more complete descriptions of reactions occurring at the solid-solution interface. The dissolution and precipitation of these rocks have been described by the net rate of equation 3-1, where the forward reaction (*kf)* is greater than the back reaction (*kb)* resulting in net dissolution of the solid (Morse and Arvidson, 2002).

(3-1) $$MeCO_3 \underset{kb}{\overset{kf}{\Leftrightarrow}} Me^{2+} + CO_3^{2-}$$

This is a simplistic representation that does not give insight into the processes occurring at the solid-solution interface, thus requiring a more comprehensive rate

equation to be developed. Empirical models were developed to give a more robust description of mineral dissolution by incorporating concepts such as distance from equilibrium, and water rock ratios (Morse and Berner, 1972). The most common representation of empirical models is described through equations 3-2 to 3-4, which outline three simultaneous reactions, which govern $MeCO_3$ dissolution (Plummer et al., 1978).

(3-2) $$MeCO_3 + H^+ \underset{Kb}{\overset{Kf}{\Leftrightarrow}} Me^{2+} + HCO_3^-$$

(3-3) $$MeCO_3 + H_2CO_3^0 \underset{Kb}{\overset{Kf}{\Leftrightarrow}} Me^{2+} + 2HCO_3^-$$

(3-4) $$MeCO_3 + H_2O \underset{Kb}{\overset{Kf}{\Leftrightarrow}} Me^{2+} + HCO_3^- + OH^-$$

Empirical models provide a strong foundation for more robust descriptions of mineral dissolution to be built upon. Variables that have been shown to impact dissolution rates include: total ions in solution (ionic strength), compositional variation of specific ions in solution, and the temperature dependence of activation energies for reactions occurring at the mineral-solution interface (Sjoberg and Rickard, 1984; Morse and Arvidson, 2002; Morse et al., 2007; Pokrovsky et al., 2009). To incorporate these variables a more accountable and comprehensive approach using surface complexation models (SCM) was put forward (Van Cappellen et al., 1993). Equations 3-5 – 3-16 outline species on dolomite surfaces where each surface site has its own activation energy (Van Cappellen et al., 1993).

(3-5) $$>CO_3H^0 \Leftrightarrow >CO_3^- + H^+$$

(3-6) $$>CO_3H^0 + Ca^{2+} \Leftrightarrow >CO_3Ca^+ + H^+$$

(3-7) $$>CaOH_2^+ \Leftrightarrow >CaO^- + H^+$$

(3-8) $>CaOH^0 \Leftrightarrow >CO_3^- + H^+$

(3-9) $>CaOH^0 + CO_2 \Leftrightarrow >CaHCO_3^0$

(3-10) $>CaOH^0 + CO_2 \Leftrightarrow >CaCO_3^- + H^+$

(3-11) $>CO_3H^0 \Leftrightarrow >CO_3^- + H^+$

(3-12) $>CO_3H^0 + Mg^{2+} \Leftrightarrow >CO_3Mg^+ + H^+$

(3-13) $>MgOH_2^+ \Leftrightarrow >MgO^- + H^+$

(3-14) $>MgOH^0 \Leftrightarrow >CO_3^- + H^+$

(3-15) $>MgOH^0 + CO_2 \Leftrightarrow >MgHCO_3^0$

(3-16) $>MgOH^0 + CO_2 \Leftrightarrow >MgCO_3^- + H^+$

SCMs allow for discrimination of multiple reactive surface sites: $>MeOH^o$ and $>CO_3H^o$ where *Me* represents a divalent metal cation (eg. Ca, Mg, Zn), which are common in naturally occurring carbonate minerals (Pokrovsky and Schott, 2002). This separation of reactive sites, allows for the rate-determining step for dissolution to be identified, allowing more rigorous dissolution models to be developed (Arakaki and Mucci, 1995; Pokrovsky et al., 1999; Liu and Wolfgang, 2001; Pokrovsky and Schott, 2001; Liu et al., 2005; Pokrovsky, et al., 2005; Pokrovsky et al., 2009). In the case of dolomite, the $>MgOH^o$ surface site has been identified as the rate-determining step; figure 3.2 illustrates the dissolution of CO_2 into the brine, exchange with the reactive surface layer, and reactions at the mineral surface.

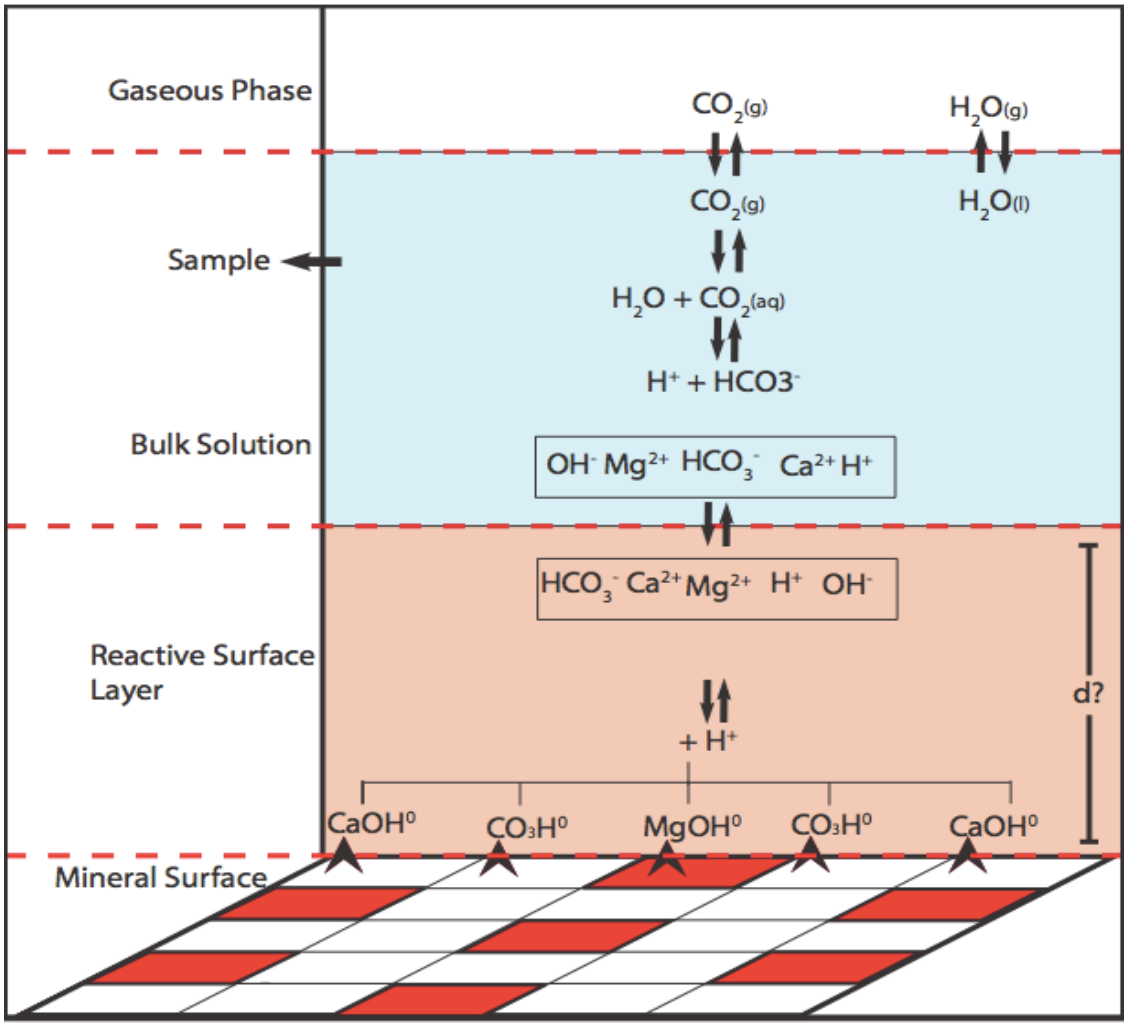

Figure 3.2: Original figure depicting chemical reactions involved in CO_2 injection into storage reservoirs is displayed for the gaseous (white), aqueous (blue), boundary layer (salmon) and solid phase (white and red). Red squares on mineral surface indicates >MgOH hydration site, which represents one quarter of surface sites.

3.1.2 Physical Controls on Dissolution Rates

CCS projects including Fort Nelson lie outside of the physical conditions that the majority of experiments on carbonate dissolution kinetics encompass. This gap may be due to experimental difficulties in working at the pressure and temperature conditions of many candidate storage sites, or perhaps to the lower relevance of high pressure-temperature carbonate dissolution studies have historically occupied (Pokrovsky et al., 2009).

The significance of physical variables such as pressure and temperature on reaction rates has been demonstrated in multiple studies. The studies investigating the temperature dependence of carbonate reaction rates (Saldi et al. 2010; Sjoberg and Rickard 1983; Pokrovsky et al., 2009) as well as mechanisms (Morse et al., 2007), have concluded that increases in temperature will increase the dissolution rates of minerals. Experiments residing in the pressure regime of CCS projects however, are less numerous (Rosenbauer et al., 2005; Bachu et al., 2007; Pokrovsky et al., 2009). Pressure has been identified in previous studies as an important variable to consider, with previous studies suggesting that failing to account for elevated pressures will lead to significant deviations between theoretical and measured mineral dissolution rates (Allen et al., 2005). It has been demonstrated for example in some recent studies that elevated pCO_2 values inhibit the rate of mineral dissolution (Pokrovsky et al., 2005; Pokrovsky et al., 2009). Salinity has been demonstrated to have a net increase in mineral dissolution rates (Finneran and Morse, 2009); constraining the effects of individual ions however remains a subject of ongoing research (Ruiz-Agudo et al., 2009; Ruiz-Agudo et al., 2011). For example it has been demonstrated that high concentrations of Mg^{2+} and HCO_3^- will act to inhibit mineral dissolution rates (Arvidson and Luttge, 2009; Pokrovsky et al., 2009).

Finally, for the purposes of CCS there is a gap in the literature with the majority of experiments being conducted on pure samples of calcite, whereas most potential carbonate storage sites are made up of Mg-bearing carbonates. Impure specimens of Mg-bearing carbonates have been demonstrated to have much lower reaction rates, and a more complex dissolution mechanism than calcite (Pokrovsky et al., 1999; Pokrovsky and Schott, 2001; Pokrovsky et al., 2005; Pokrovsky et al., 2009; Schott et al., 2009; Saldi et al., 2010). All of the parameters mentioned here are important but often difficult to

accurately apply in mathematical extrapolation tools. This makes experimentation paramount in the development of better geochemical models for CCS.

3.1.3 Overview

The objectives of this work are explored through three central inquiries. The first objective is to determine of the dissolution rates of the Keg River formation in response to CO_2 injection. Second a comparison of the dissolution rates of the Keg River formation rock in natural brine versus simplified synthetic ones. And finally to investigate the specific effects that ions Zn^{2+} and Sr^{2+} exert on Keg River formation dissolution rates. This work provides reaction rate data, which would best serve as the foundation for future reactive transport simulations of the Fort Nelson CCS project.

3.2 Materials and Methods

Dolomite dissolution can be described by equation 3-17 (Pokrovsky et al., 2009) where the reaction rate R of solids dissolving into solution in response to CO_2 injection, is a function of the change in the measured value of ion Me^{2+} in the solution over time t; the product of the temporal change in the concentration of species Me^{2+} is then divided by the calculated reactive surface area A_x, which gives the rate of reaction per area of solid that is available to react. This equation would be sufficient in a flow through system where concentrations of ions in solution are never permitted to reach saturation and instead remain in a steady state. In a closed system however a power law must be used to interpret rate data (equation 3-18), where a rate constant K is determined along with an exponential factor n. Note in equations 3-17 and 3-18 R is equal to K.

(3-17) $R = (d[Me^{2+}]/dt)/A_x$

(3-18) $[Me^{2+}]=Kt^{n}/A_{x}$

This section will describe the materials used in experiments, and outline the methods used to quantitatively measure *K* and *n* through experiments involving measurements of both Me^{2+} and A_x.

3.2.1 Materials

Rocks collected from the Keg River formation consist of approximately 93% dolomite, 5% calcite and 2% quartz (Table 2.2). Solid material used in the experiments were taken from the Keg River formation in the Fort Nelson area as drill chips, which were then ground in a ring mill and passed through a No. 200 sieve to isolate the sub 75 μm fraction. After sieving, samples were soaked in deioniozed MilliQ® (18.2 MΩ) water for 1 hour to remove fine particulates residing on mineral surfaces. Figure 3.3 displays SEM images of carbonate grains used in experiments.

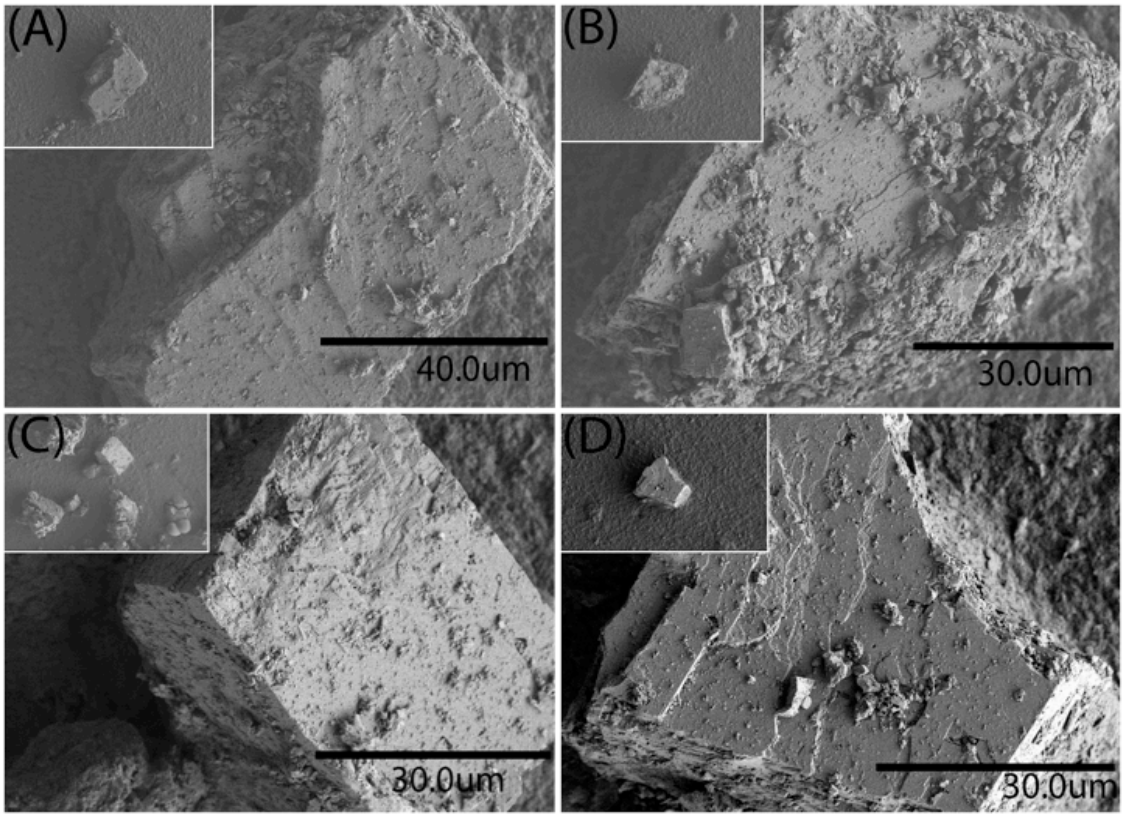

Figure 3.3: Scanning electron microscope images with the electron beam set at 1 kV of Keg River carbonate grains, taken at the University of Victoria. Images (A) through (D) are displayed with both a zoomed in and zoomed out (upper right) images of grains. Note both the quadralateral surfaces and the large degree of surface roughness particularly in image (B).

Both a natural and a synthetic fluid were used in experiments. As summarized in section 2.2.1, natural brines were collected from the Keg River formation in May 2009. A full summary of Keg River brine composition is provided in section 2.4.3, where it is shown that ions Cl^-, Na^+, Ca^{2+}, K^+, HCO^-, S, and Mg^{2+} make up the majority of the bulk brine chemistry. This composition is the basis used to create synthetic brines (Table 3.1). Synthetic brines were made gravimetrically from stock materials, where solids were dissolved into 4.000 L of deioniozed MilliQ® (18.2 MΩ) water, and over several hours dissolved by a magnetic stirrer at 80 °C. Small amounts of HCl were added to synthetic brines to reach the pH values measured in Keg River brines -approximately 6.5.

Table 3.1 Bulk Fluid compositions of synthetic brines compared to natural Keg River brine.

Ion (mmol)	DK-1 – DK-4	DS-1 – DS-8	DS-9	DS-10
Cl^-	262	262	262	262
Na^+	230	230	230	230
Ca^{2+}	25.0	25.0	19.9	19.1
HCO_3^-	24.6	24.6	24.6	24.6
K^+	15.0	15.0	15.0	15.0
SO_4^{2-}	5.20	5.20	5.20	5.20
Mg^{2+}	5.0	5.0	5.0	5.0
Sr^{2+}	0.9	0.00	10.0	0.00
Zn^{2+}	0.1	0.00	0.00	10.0

3.2.2 Experimental Set up

A picture of the experimental apparatus and a full schematic is displayed in figures 3.4 and 3.5. A 600 mL Parr® T316 stainless steel non-stirred high-pressure reactor vessel, capable of reaching temperatures and pressures of 350 °C, and 190 bar respectively, housed the model aquifer.

Figure 3.4: Image of experimental apparatus used for dissolution experiments.

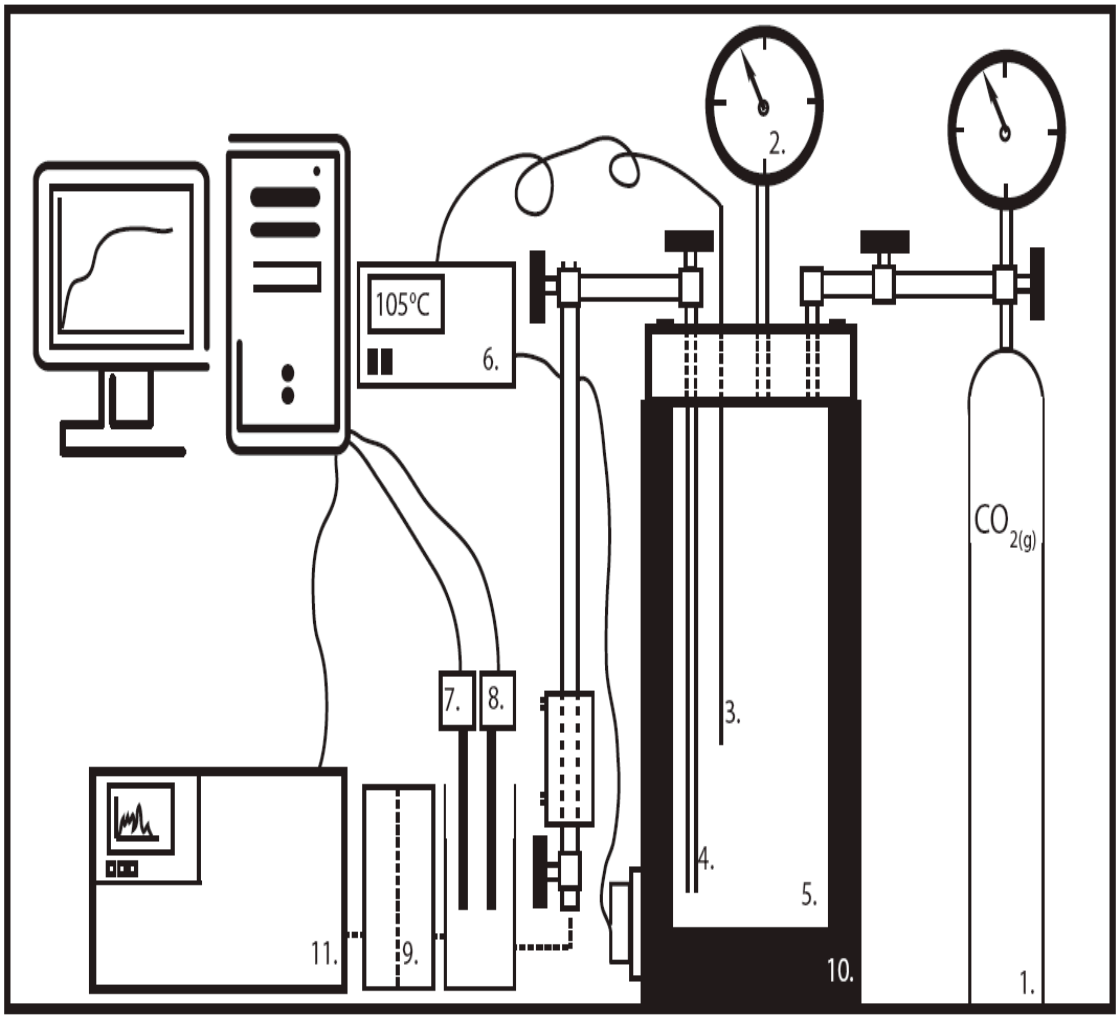

Figure 3.5: Representative schematic of the experimental set up utilized in this work: (1) CO_2 cylinder, (2) manometer, (3) thermocouple, (4) dip tube, (5) reactor vessel, (6) temperature controller, (7) pH meter, (8) conductivity meter, (9) 0.200μm filtering membrane, (10) heating mantle, (11) Various fluid analysis.

Temperature was raised to reservoir conditions with a 700 Watt, 115 V Parr® A2230HC3EB bench top heater moderated with a 115 V Parr® 4838EB temperature controller and attached to a thermocouple located within the reactor vessel. Pressure was induced directly from a CO_2 cylinder and measured with a manometer located on the head of the reactor. In order to sample directly from the reactor during experiments, the reactor was outfitted with a dip tube connected to an outlet and needle valve at its base (Figure 3.5). The base of the sampling port was outfitted with a cooling jacket to allow water to

circulate in order to rapidly return the sample temperature back to ambient conditions (25 °C).

Experiments were conducted at 105 °C (reservoir conditions) and at a pressure of 50 bar pCO_2. The lower-than-reservoir pressures allowed for rapid sampling immediately after CO_2 injection at 105 °C, while still placing the CO_2 phase under high pressure conditions. Higher pressures would have required either the introduction of solid CO_2 (dry ice) or the immediate injection of gaseous CO_2 before the reactor was heated; both of these scenarios would have fundamentally changed where reactions occurred. An example of this is in the case of dry ice, where solid CO_2 would be in contact with mineral samples at the base of the reactor, which may have frozen and broke up some grains. Both of these methods of increasing pCO_2 would have limited sampling times of the reactor to post CO_2 injection where immediate sampling could only occur before the fluids had reached the target temperature of 105 °C. This would have missed the most rapid dissolution period in the reactor (0-100 min) and thus lower the confidence in results.

To avoid artificially accelerated reaction rates, rock powders were immersed in the brine for 24 hours at 105 °C before experiments commenced, to allow impurities to adsorb onto mineral surfaces as would be the case within natural formations (Eisenlohr et al., 1999). Each experiment involved approximately 12.5 g of rock loaded at the bottom of the reactor and approximately 500 mL of natural or synthetic brine poured on top of the solid phase and stirred. This created a water-rock ratio for experiments of 40:1 by mass. This amount of rock was chosen for experiments with the knowledge that it would be in excess of the surface area available to react. Maximization of water rock contact

allows for the maximum potential for diffusion of ions to move through the boundary layer *d* into the bulk solution (Figure 3.2) thus providing maximum *R and K* estimates that are useful for constraining the upper limit of injection scenarios. Initial experiments were run over 10000 minutes but were decreased to 500-1000 minutes, which allowed for more samples to be taken prior to equilibrium when the most rapid dissolution kinetics occur. In order to insure homogeneity within the reactor vessel, it was manually agitated at 30 minute intervals for 1 minute by rapidly rotating the reactor 90° and back. This ensured any stratification to be broken down within the 100-300 minute sampling intervals. Results for tests of homogeneity show that indeed there is very little variation within the reactor, and that fluids are homogeneous (Appendix II).

There are important differences between the experimental set up outlined for this work and that of natural systems. The scale and complexity of the Keg River and other geologic formations proposed for CO_2 storage are not reproducible in the laboratory. It is also impossible to experiment over the time scales of CCS projects (100-1000s of years). Finally, conditions of the Keg River formation are difficult to confidently scale down to laboratory sized reactors as target formations will be heterogeneous and flow regimes in carbonate formations will be a combination of intrinsic and fracture porosity and permeability. For this reason, a set up was chosen that will represent maximum *R* and *K* values but minimize this maximum by using natural samples of rock and brine as opposed to the common practice in the literature.

3.2.3 Real-time Solution Analysis

Utilization of the dip tube and needle valve (Figure 3.5) allowed real time changes in solution chemistry to be followed through measurements of pH, conductivity and

alkalinity. In order to ensure accurate sampling of the bulk fluid present in the reactor at the sampling time, 5 mL of fluid was purged to flush out residual brine left in the dip tube from the previous sample, leaving a net loss of fluid volume in the reactor of 10 mL per sample. All water analyses were made at near-ambient conditions to dampen rapid exsolution of CO_2 from the fluid, and to ensure that measurements using pH, and conductivity meters were made within manufacturers' recommended operating parameters.

Alkalinity measurements were made with a Hach digital titration kit; as described in Section 2.2.5 of this thesis. pH measurements were made using a Fisher Scientific® Accumet pH meter with a standard glass electrode. Conductivity measurements were made with an Omega® Pocket Pal conductivity meter with an accuracy of (±) 1% over a range of values from 0-200,000 μS. Calibrations of both pH and conductivity were made before and after sample analysis. The pH meter was calibrated with three NIST certified Oakton® buffers (pH = 4.01, 7.0, and 10.0) with an accuracy (±) 0.01 pH units, and auto corrected to 25 °C; calibrations for conductivity were made with standards CDSA 450, 4500, and 45000, which are all NIST certified KCl solutions. Both pH and conductivity was measured directly out of the sampling port, however, additional conductivity measurements were made after filtering through a 0.200 μm membrane and were then diluted 100 times. Some alkalinity measurements were made directly out of the sampling port at 25 °C, although some experiments required measurements to be made after experiments were completed, which did not impact final results.

3.2.4 Ex-situ Solution Analysis

Upon completion of experiments, water samples were analyzed for major and minor cation and anion constituents. Section 2.3.5 outlines the methods used for natural brines, however a small addendum is required to describe synthetic brine analysis. Major and minor cation and anion analysis for all experiments involving synthetic brines occurred at Acme Analytical Laboratories in Vancouver, British Columbia. Analysis was performed using an ICPMS, with replicate analysis of standard reference material TDMA-70 to determine the accuracy and precision. Values varied dependent upon the analyte but were comparable to results from analysis conducted at the University of Victoria.

3.2.5 Surface Area Analysis

The surface area of solid materials was quantified using two methods. First, geometric surface area (A_{GEO}) was calculated by measuring 137 individual grain edges (Figure 3.6) from SEM images, which were then inserted into equations 3-18 to 3-23 (Gledhill, 2005).

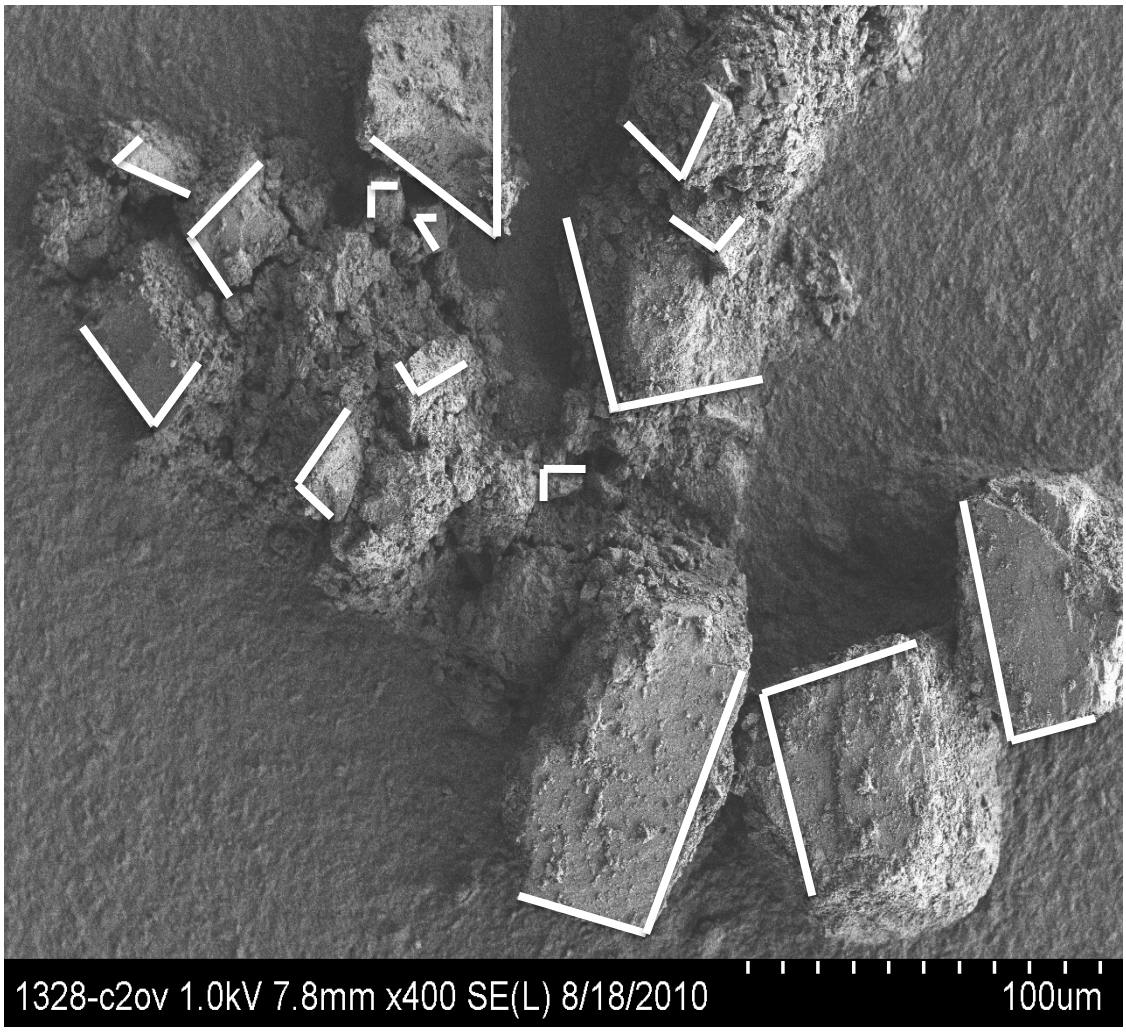

Figure 3.6: Hitachi® S-4800 field emission scanning electron microscope images with the electron beam set at 1 kV of Keg River carbonate grains, taken at the University of Victoria. Grain edges are highlighted in white and were used to calculate the geometric surface area of rock powders used in experiments.

(3-18) $A_{GEO} = \Sigma_j A_j m_f$

(3-19) $A_j = (6l^2/pl^3) = (6/p)l^{-1} \times 10^{-4}$

(3-20) $m_f = (m_j/m_T)$

(3-21) $m_j = pl^3$

(3-22) $m_T = \Sigma_j m_j$

A_x represents the surface area per gram of grain x, and m_f is the mass fraction. The edge length is represented by l, and the density of the solid by ρ ; m_x represents the mass of grain x and m_T is the total mass. An underlying assumption in this method was that

grains are contained within a rhombohedral geometry. Specific surface area was determined by N_2 gas sorption, BET analysis (Brunauer et al., 1938). Sample masses of approximately 6 g were loaded into a Quantacrome® Autosorb automated gas sorption system and outgassed for 7 hours at 50 °C. These two methods were within 10% of one another with a geometric surface area measured at 1.394 $m^2 \cdot g^{-1}$ and a specific surface area measured at 1.287 $m^2 \cdot g^{-1}$ suggesting high confidence in the surface area of solids used in this study.

Knowledge of the surface area of solids used in experiments is important in order to determine reaction rates. This was achieved by stoichiometrically combining the total amounts of Mg^{2+} and Ca^{2+} released to solution and measured in experiments to CO_3^{2-} and calculating the total rock mass reacted.

Another important question is what surface area of rock is actually reacting in experiments? This is a complicated question and has been the topic of a number of studies (Fischer and Gaupp, 2004). The Keg River work calibrated experiments through conductivity measurements from experiments using synthetic brines made to replicate Keg River brine with variable amounts of solid mass. The assumption was made that increases in conductivity were due to the release of ions to solution from dissolving minerals. Increases in the dissolution rate were found to correlate with the amount of solid in the reactor vessel. Data presented show a maximum of approximately 0.1g can react at one time no matter how much solid is placed in the reactor (Figure 3.7). Results are thus presented in terms of rate of release of ions to solution per mass of material that reacted which can also be presented as a release of ions per unit of available surface area

to react (Figure 3.7). A full table of data from these experiments is presented in Appendix III.

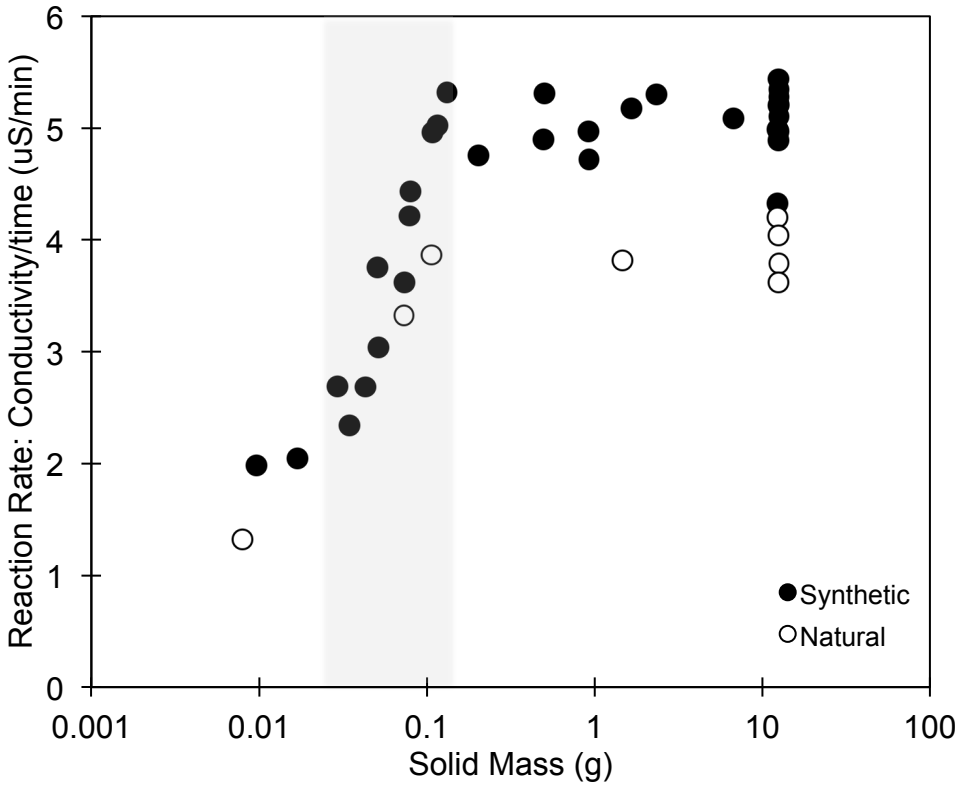

Figure 3.7: Reactive surface area calibration in natural (open circles) and synthetic (solid circles) brines, measured as a function of changes in conductivity versus mass of reacting rock. Note the mass independent regions between 0–0.01g and 0.1-12.7g and the mass dependent region highlighted in grey between 0.01-0.1g. Measured reaction rates were normalized to a reacting rock mass of 0.1g.

3.3 Results

A summary of reaction rates and experiments is given in table 3.2 and a full table of raw data is given in Appendix IV. Results here are measurements of natural Keg River brine in experiments at near formation conditions. Subsequent experiments are performed on synthetic brines to increase confidence in experimental reproducibility, evaluate the validity of synthetic brines in extrapolating to natural systems, and to increase the existing data set for the carbonate system.

Table 3.2: Geochemical results for experiments DK-1 – DK-4 and DS-1 – DS-10, simulating CO_2 injection for the Fort Nelson CCS Project. All Experiments were conducted with Keg River Formation rock. Values in red were removed after Q-testing at the 90% confidence interval. Error represents the maximum deviation from the experimental mean, which encompasses the total experimental and analytical error.

Exp. ID	Fluid	pH	Salinity /mmol	[Ca] /mmol	[Mg] /mmol	Log K_{Ca}	n_{Ca}	Log K_{Mg}	n_{Mg}
DK-1	KR	6.2-5.4	0.4	22-27	4.7-5.2	-9.30	0.78	-10.12	0.81
DK-2	KR	6.4-5.6	0.3-0.4	25-30	4.9-5.5	-9.25	0.82	-9.80	0.74
DK-3	KR	6.3-5.4	0.4	24-28	4.9-5.4	-9.29	0.81	-9.82	0.74
DK-4	KR	6.5-5.6	0.4	24-29	5.1-5.6	-9.30	0.81	-9.80	0.74
DKavg	KR	6.4-5.5	0.4	24-28	4.9-5.4	-9.29 ±.04	0.81	-9.80 ±.02	0.74
DS-1	Syn	6.8-5.7	0.3-0.4	24-26	5.1-6.7	-9.44	0.79	-11.3	0.57
DS-2	Syn	6.4-5.3	0.3-0.4	27-31	5.0-6.6	-9.34	0.81	-9.44	0.79
DS-3	Syn	6.4-5.5	0.3-0.4	26-32	5.0-6.8	-9.17	0.83	-9.40	0.79
DS-4	Syn	6.4-5.4	0.3-0.4	25-32	5.0-6.8	-9.12	0.83	-9.40	0.79
DS-5	Syn	6.3-5.3	0.3-0.4	25-32	5.1-6.6	-9.15	0.83	-9.41	0.79
DS-6	Syn	6.4-5.5	0.3-0.4	26-32	5.0-6.7	-9.32	0.81	-9.43	0.79
DS-7	Syn	6.6-5.3	0.3-0.4	26-32	5.1-6.8	-9.23	0.82	-9.44	0.79
DS-8	Syn	6.4-5.5	0.3-0.4	25-31	5.2-6.6	-10.48	0.67	-9.52	0.78
DSavg	Syn	6.5-5.5	0.3-0.4	25-31	5.1-6.7	-9.23 ±.21	0.82	-9.43 ±.09	0.79
DS-9	Sr-Syn	6.5-5.3	0.3	19-24	5.1-6.0	-9.30 ±.21	0.81	-9.67 ±.09	0.76
DS-10	Zn-Syn	6.3-5.6	0.3	26-28	5.1-7.2	-9.15 ±.21	0.83	-9.43 ±.09	0.79

Errors: pH ± 0.01, Salinity ± 0.05, [Ca] ± 0.5, [Mg] ± .05

3.3.1 Changes in Brine Chemistry upon CO_2 Injection

The model aquifer in these experiments responded to CO_2 injection by changes in solution chemistry and mass of solid. Upon CO_2 injection into natural brines (DK-1 – DK-4), the pH of the solution immediately dropped from approximately 6.2 to below 5.4

(Figure 3.8). This effectively moved the system out of the pseudo equilibrium established from years of communication between aqueous and solid phases present in the Keg River formation. This drop in pH was due to the production of carbonic acid where CO_2 is converted to HCO_3^- and H^+. The solids dissolve due to this increase in acidity, which then moves the system toward a new equilibrium, as observed by increases of conductivity (Figure 3.8), carbonate species (Figure 3.9), and Mg^{2+}, and Ca^{2+} (Figure 3.10). The data generated in these experiments outline two distinct regions of reactions: first a region of rapid change approximately 0-1000 minutes (far from equilibrium), and second a region of apparent stabilization 1000 – 5000 minutes (near equilibrium). The subsequent work on this system focuses on the 0-1000 minute period where the most rapid geochemical changes to the system occur. In a full-scale CCS project this time interval represents the CO_2 injection period.

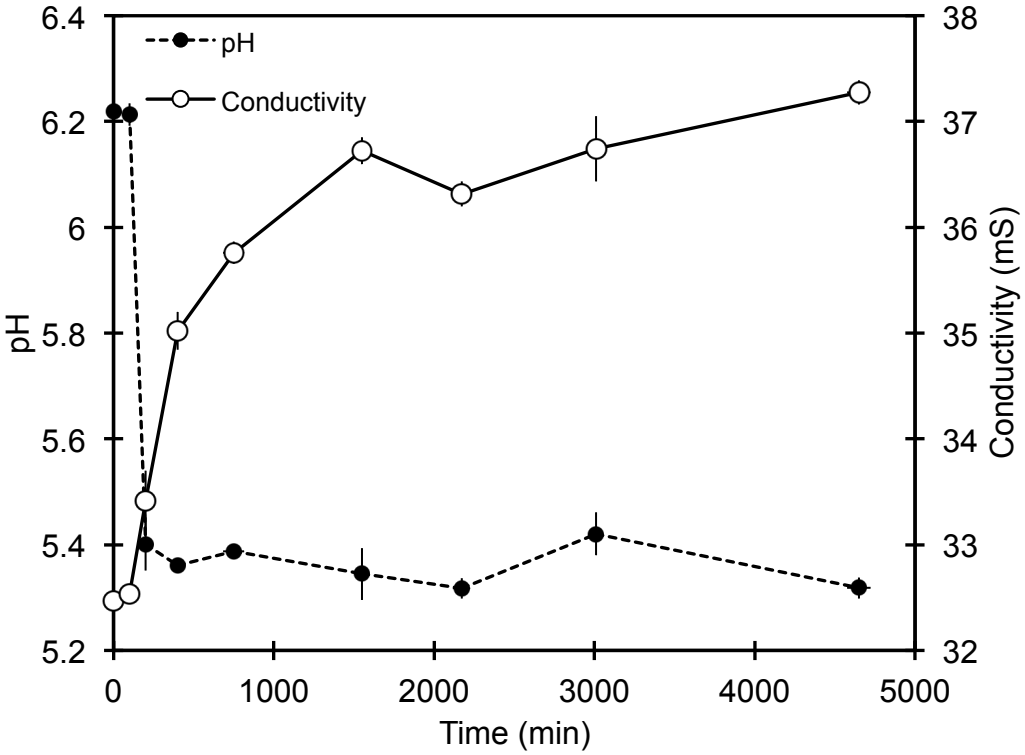

Figure 3.8: Conductivity (in milli-siemens) and pH evolution of natural brines for the average value of experiments DK-1 – DK-4. Error bars represent the standard deviation of four replicate experiments. CO_2 injection occurred at time = 100 minutes.

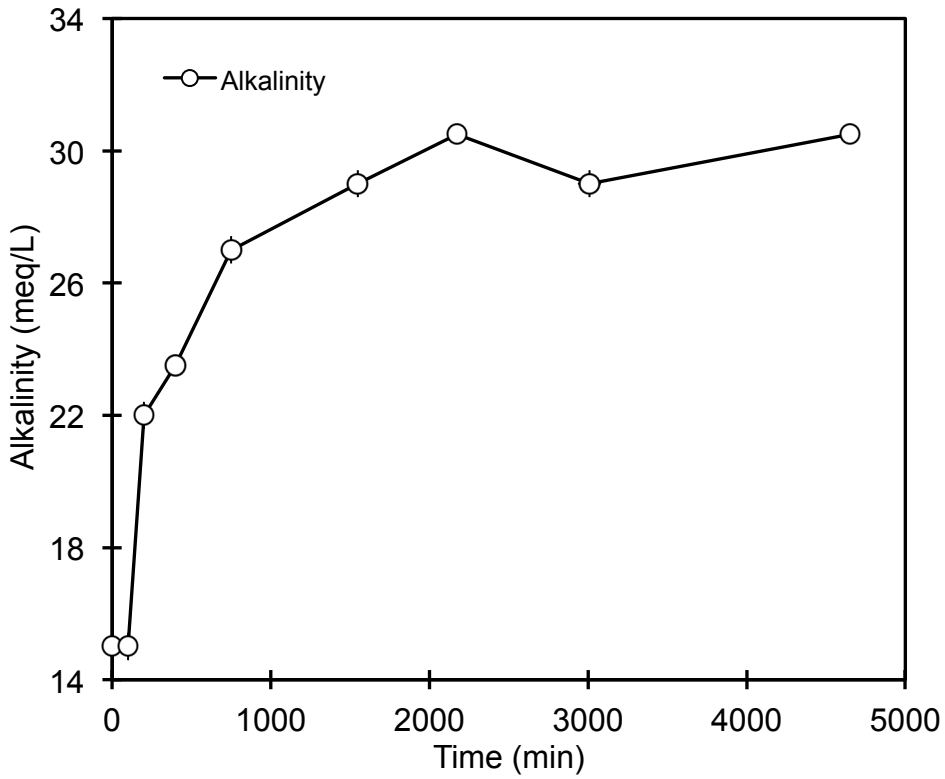

Figure 3.9: Averaged alkalinity measurements taken by digital titration of H_2SO_4 into natural brines for experiments DK-1 – DK-4. Error bars represent the standard deviation of four replicate experiments. CO_2 injection occurred at time = 100 minutes.

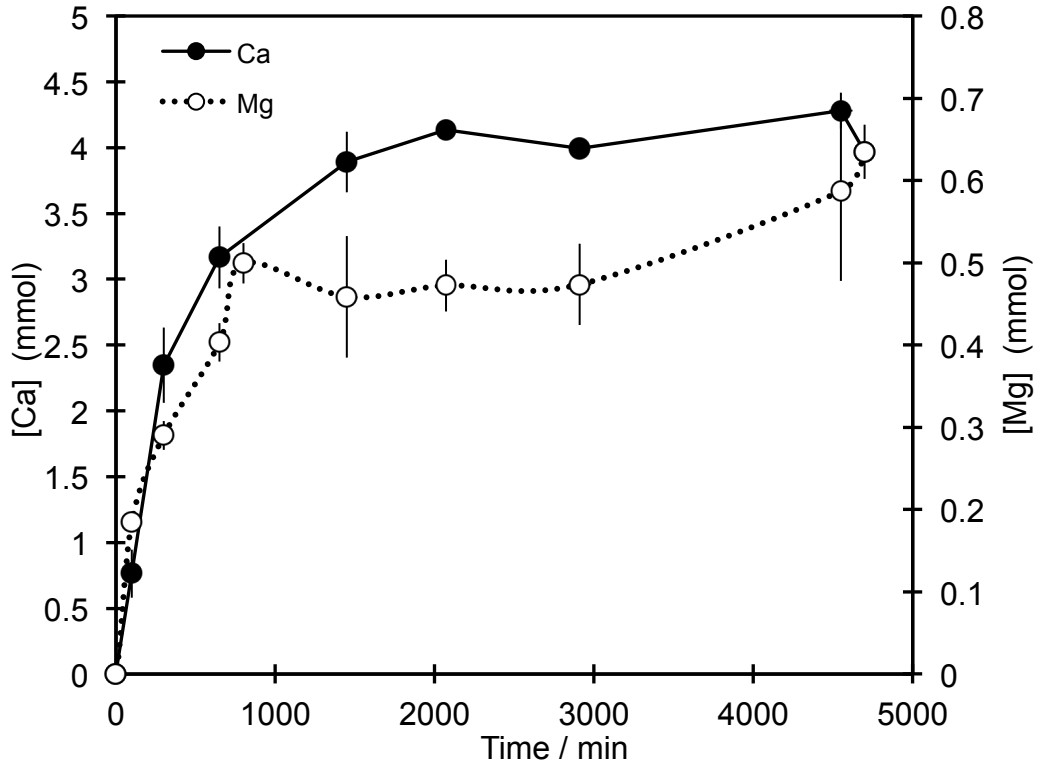

Figure 3.10: Averaged concentrations of Ca and Mg over time, at 50 bar pCO_2 and 105 °C for Experiments DK-1 – DK-4. Error bars reflect standard deviations for four replicate experiments. CO_2 injection occurred at time = 0 minutes.

3.3.2 Experimental and Analytical Reproducibility

Experiments conducted were rigorously checked for both analytical and experimental reproducibility. Stratification of the fluid within the reactor was identified as a potential problem, which would be expressed in the data as measured values of ions, only representing a portion of the fluid in the reactor. This would render calculated reaction rates or rate constants inaccurate. To overcome any stratification in the fluid the reactor was agitated every 30 minutes during experiments. The effectiveness of this approach was tested by two trial runs where the entire reactor was evacuated and measured for major cations. No significant variations in cation concentrations were found throughout a vertical column in the reactor (Appendix II).

Next the reproducibility of data points was tested through replicate experiments under the same pressure and temperature conditions for both natural and synthetic brines. Natural brines were run four times and synthetic brines eight times at 50 bar pCO_2 and 105 °C. Trends were found for changes in both Ca and Mg concentrations with time, which were concluded as being statistically significant as the magnitudes of the change in species concentrations greatly exceeded the standard deviations of any individual data points.

Finally, because different methods were used in measuring cation concentrations of different experiments, samples from experiment DK-1 were measured on both IC and ICPMS (Appendix V). Results were similar, only differing a maximum of 10% between the two methods with elevated values of Ca measured in the ICPMS. Comparison of analysis between the University of Victoria, and Acme Analytical was not performed due to limited sample availability.

3.3.3 Metal Release and Dissolution Rates

Metals released into solution upon CO_2 injection, was done so incongruently with different metals released in different quantities, for example Sr^{2+}, and Zn^{2+}, are released at far greater concentrations than other trace metals (Figure 3.11). This shows how impurities within natural minerals will participate in geochemical changes in reservoir brine, induced by injecting CO_2.

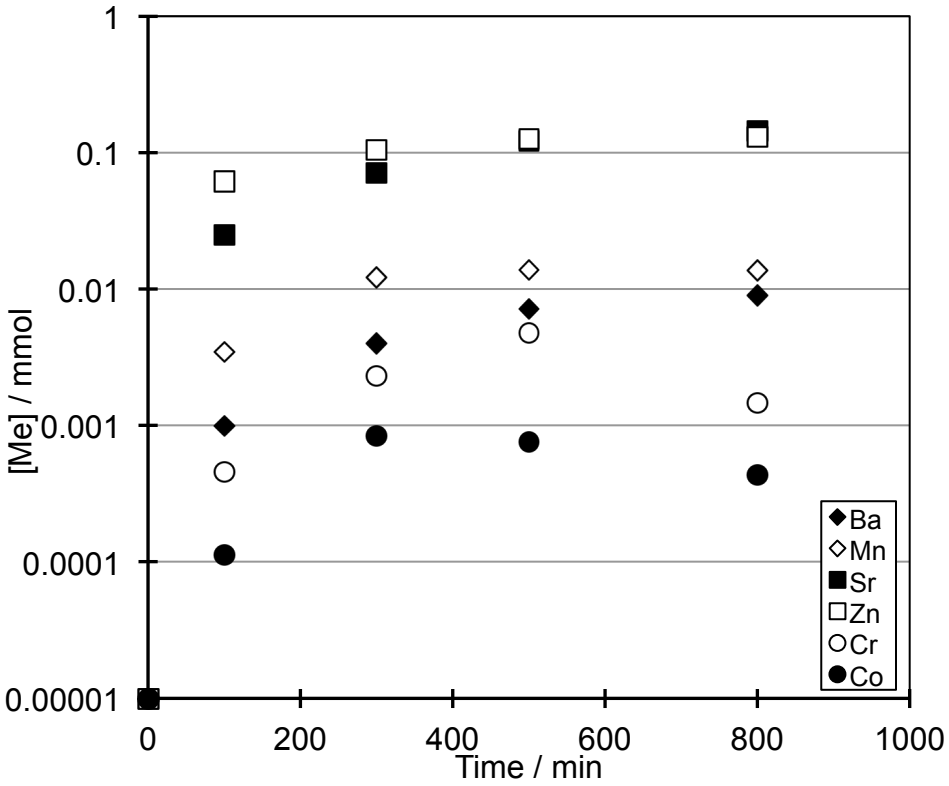

Figure 3.11: This figure depicts incongruent dissolution of carbonate surfaces. This is demonstrated through the release of trace metals Ba, Mn, Sr, Zn, Cr and Co at different quantities from carbonate surfaces for experiment DK-1, at 50 bar pCO_2 and 105 °C.

Similar to previous work Ca is released in a larger quantity and at a higher rate than Mg for two reasons: first Ca build up on dolomite surfaces, and second the longer bond length between Ca and C in the dolomite structure allows it to be removed with a lower energy cost than Mg (Arvidson et al., 2006; Schott et al., 2009). Another possibility is that the carbonates reacting were non-stoichiometric, in that there were greater amounts of Ca than Mg in the mineral lattice.

Arrhenius plots were constructed from experiments at 50 °C, 105 °C, and 200 °C and 50 bar pCO_2, (Appendix VI). Due to the experimental uncertainty in the data, these experiments will not be discussed further in this work. It is important to note however, that results presented here were found to have consistent trends with previous studies,

with increases in reaction rates up to 100 °C and then decreases up to 200 °C (Pokrovsky et al., 2005; Pokrovsky et al., 2009).

Experiments conducted on natural and synthetic brines at the same experimental conditions (105 °C, 50 bar pCO_2), yielded different rate constants (*K*) and exponential factor values (*n*). Comparing the initial release of Ca from mineral surfaces, it is shown that in synthetic brines Ca is released from surfaces at a higher rate than natural brines (Figure 3.12). Mg release is even more sensitive to changes in brine chemistry; Mg ions are released from synthetic brines with rate constants over 120% larger than natural (Figure 3.13). This data outlines the importance of the full suite of ions that exist in natural brines in controlling the dissolution of carbonates.

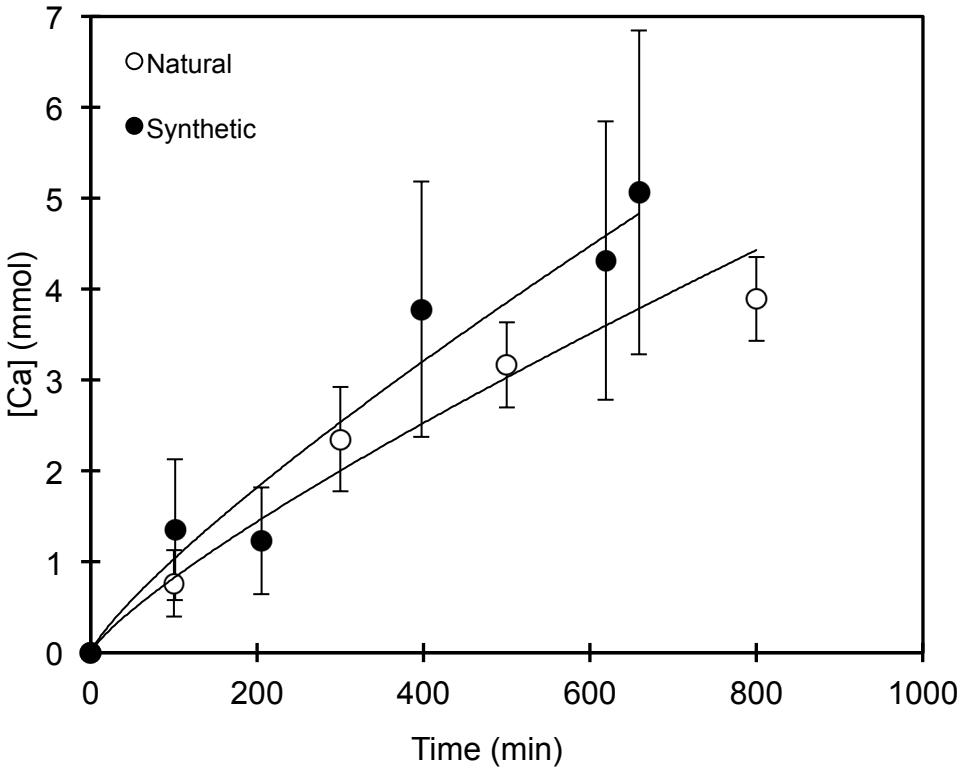

Figure 3.12: Average Ca release rate from experiments involving natural brines (DK-1 - DK-4) and synthetic brines (DS-1 – DS-8) at 50 bar pCO_2 and 105 °C. Error Bars are presented as standard deviations.

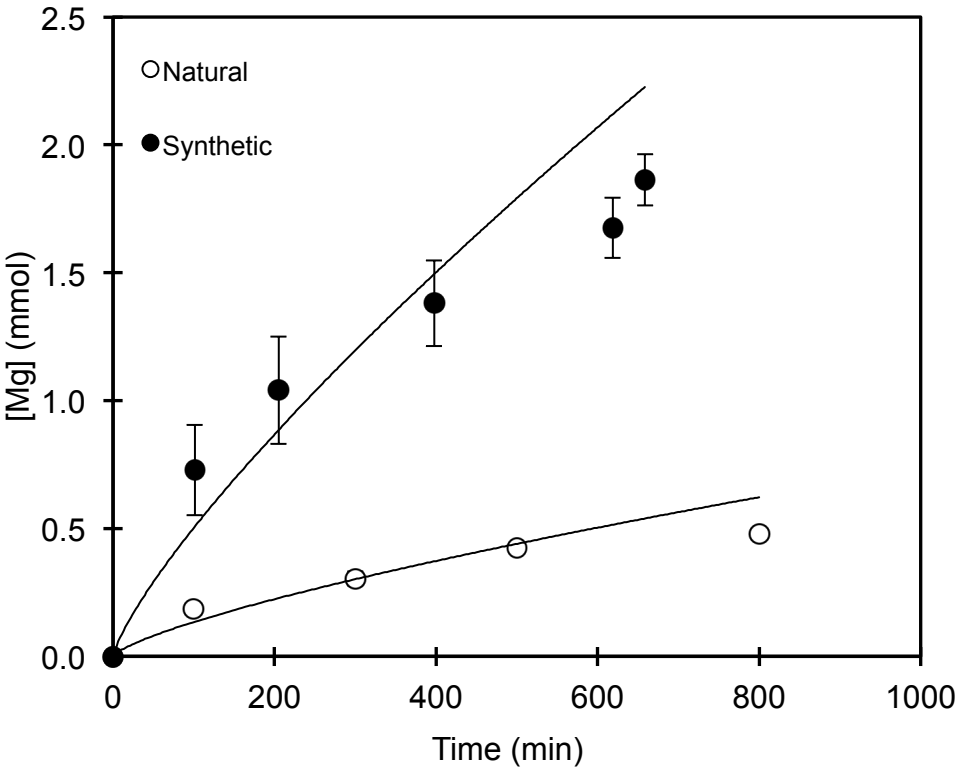

Figure 3.13: Averaged Mg release rate from experiments involving natural brines (DK-1 - DK-4) and synthetic brines (DS-1 – DS-8) at 50 bar pCO_2 and 105 °C. Error Bars are presented as standard deviations.

3.3.4 Trace Metal Behaviour

To test the effects of individual ions on dissolution rates, synthetic brines were prepared with the addition of ions Sr^{2+} (DS-10), and Zn^{2+} (DS-9), at approximately 10 $mmol \cdot L^{-1}$ concentration. Changes in the rate of release of Ca^{2+}, due to the addition of these ions to solution was not observed (Table 3.2) (Figure 3.14). Mg^{2+} release was different however, with a strong influence of Zn^{2+} reducing the rate of Mg^{2+} release by approximately half (Figure 3.15). A slight elevation of Mg^{2+} release was observed in brine containing Sr^{2+}, however more trials are needed to determine if this is statistically significant.

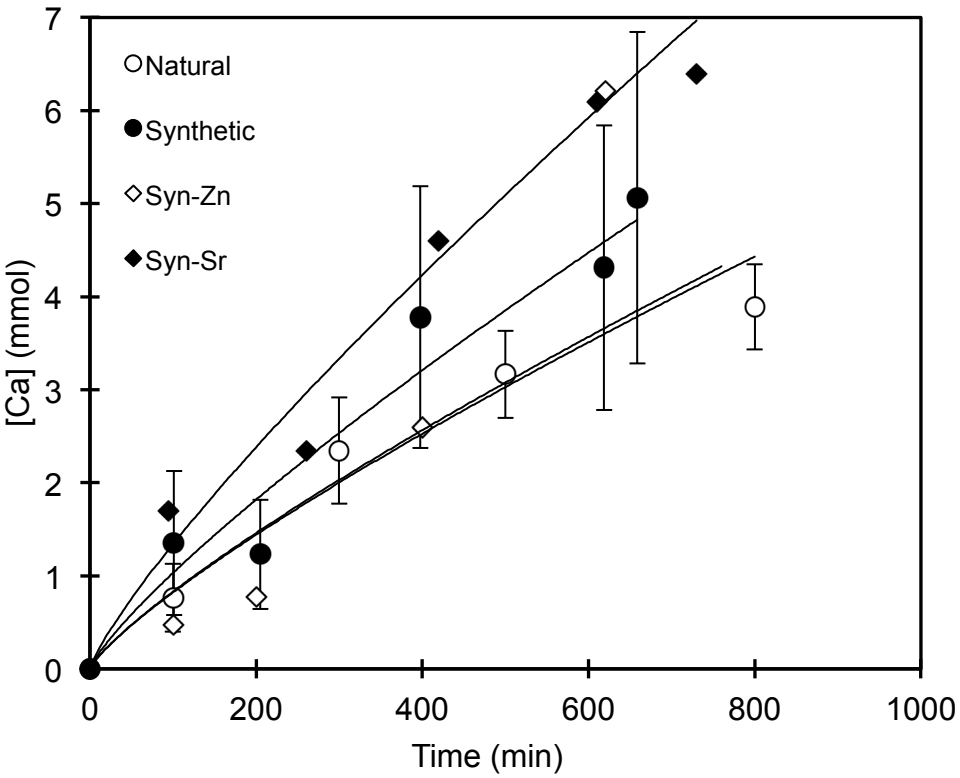

Figure 3.14: Release rate of Ca in synthetic brines for experiments with synthetic brines DS-1 – DS-8, DS-9 (Sr spiked), and DS-10 (Zn spiked), and natural brines (DK-1 – DK4) at 50 bar pCO_2 and 105 °C. Error bars on data points represent standard deviations for synthetic and natural brines.

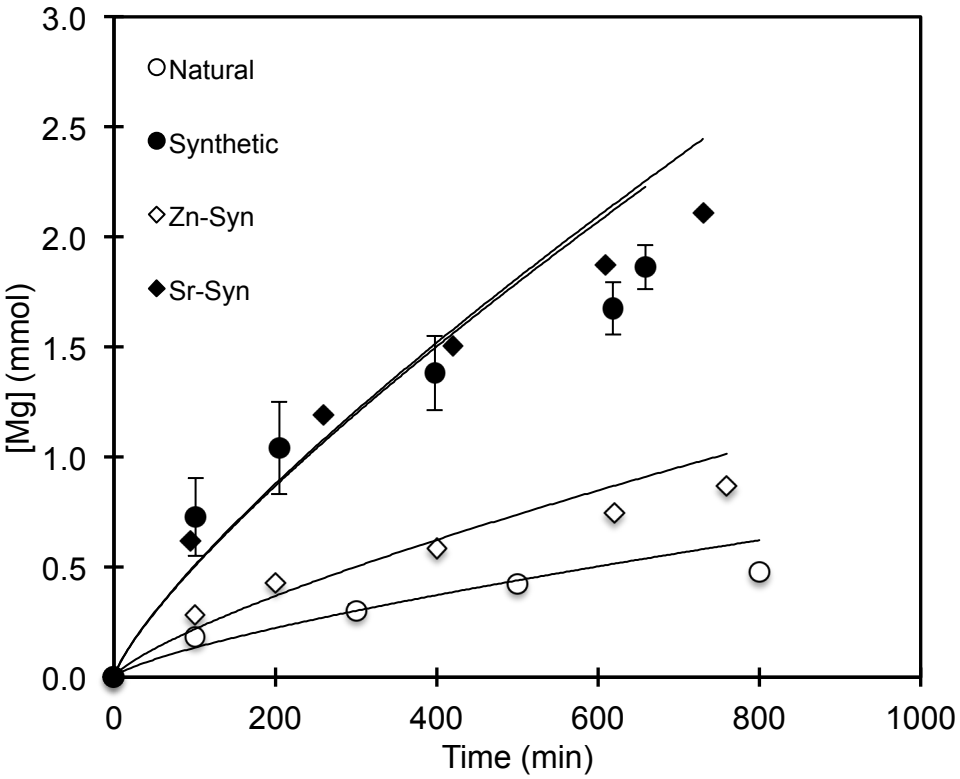

Figure 3.14: Release rate of Mg in synthetic brines for experiments DS-1 - DS-8, DS-9 (Sr spiked), and DS-10 (Zn spiked) at 50 bar pCO_2 and 105°C. Error bars are presented as standard deviations for experiments DS-1 – DS-8, and DK-1 – DK-4.

3.4 Discussion

3.4.1 Fluid Evolution in the Keg River Formation

It was not surprising that upon CO_2 injection, a drop in pCO_2 measured on the manometer indicated that CO_2 dissolved into the brine where it initiated chemical reactions. This CO_2 reacted with the fluid to produce HCO_3^- and H^+. This increase in solution acidity moved dolomite –the dominant lithology- from super-saturated to under-saturated, which then initiated dissolution of formation rock measured through the release of Ca^{2+} and Mg^{2+}. The salient findings of this chapter are as follows:

1. The dissolution rates measured in this work are consistent with previously measured values of similar fluids and rock placed under similar pressure and temperature conditions (Pokrovsky et al., 2005; Pokrovsky et al.,2009) (Table3.3).

2. Natural brines show significantly reduced dissolution rates from synthetic brines of the same major chemical constituents.

3. Individual ions of mmol concentration can produce very large impacts on dissolution rates despite similar size and oxidation states (Figure 3.13 and 3.14).

3.4.2 Dissolution Rates in Keg River

The carbonate dissolution rate constants measured for the Keg River formation materials in experiments were Log K = -9.80 ±0.02 where K was calculated with units $mol \cdot cm^{-2} \cdot s^{-1}$. This rate was averaged from four experimental runs at pCO_2 of 50 bar, and a temperature of 105 °C and calculated based on the rate of release of Mg^{2+} into solution. At this rate, assuming that the far from equilibrium region persisted for approximately 1000 minutes, over the course of experiments approximately 0.12 g of solid dissolved which means approximately 1% of rock in the Keg River formation could potentially dissolve to compensate for CO_2 injection. To put this into context, previous work has found the porosity of the Keg River formation to be between 6-25% (Sorensen, 2010); results presented here posit that CO_2 injection into the Keg River formation could increase the porosity of the formation by 4-17%.

Solids used did not dissolve congruently or stoichiometricaly with the rate of release of Ca^{2+} of Log K = -9.29 ±0.04, which is over three factors greater than that of Mg^{2+} release to solution. The non-stoichiometric dissolution of the predominantly dolomite formation rocks has multiple explanations. This phenomenon may be due to differences between the Ca and Mg concentrations in solution and solid phases, their intrinsic atomic properties, and different concentrations in the mineral lattice. The stoichiometry of the solids used in experiments is not thought to be a significant factor

because the Devonian carbonates used, are broadly considered to be near stoichiometric (Lumsden and Lloyd, 2008). Furthermore detailed atomic composition analysis on minerals used in this work was not conducted, and therefore will not be discussed further. The differences between Ca and Mg impact mineral surfaces in a number of ways including mode of dissolution and ion exchange reactions (Lumsden and Lloyd, 2008). Multiple studies propose that the hydration of the >MgOH binding site is the rate-determining step in dolomite dissolution (Pokrovsky et al., 2005) due to the difference in bond lengths between Ca-O (0.236 pm) and Mg-O (0.210 pm) (Schott et al., 2009), requiring different hydration enthalpies to break this bond to release Mg^{2+} to solution (Arvidson et al., 2006). This is expressed in experiments through the preferential release of Ca^{2+} at both a higher rate and larger quantity than Mg^{2+}, and has been demonstrated through previous studies, including this one (Paquette and Reeder, 1995; Schott et al., 2009). Formation of a Ca-rich layer on dolomite has also been simulated in atomistic models (Titiloye et al., 1998); both of these factors contribute to elevated Ca^{2+} release into solution.

3.4.3 Comparative Analysis

Previous studies on the dissolution kinetics of carbonate rocks (Herman and White, 1985; Pokrovsky et al., 1999; Liu and Wolfgang, 2001; Pokrovsky and Schott, 2001; Pokrovsky and Schott ,2002; Liu et al., 2005), have put forward a number of explanations for the rates they measured, which vary over pressure, temperature, solution and rock composition parameters, and even between studies under similar reported conditions (Table 3.3). Recent studies have started to investigate these reactions in the pressure, and temperature region that will be experienced in CO_2 storage reservoirs

(Pokrovsky et al., 2005; Rosenbauer et al., 2005; Pokrovsky et al., 2009). Prior to these investigations, no published studies investigated dissolution kinetics of carbonates at pCO_2 values greater than 1 bar. Rates Log K = -9.80 ±0.02 measured in this work are consistent with previous studies (Table 3.3.) Log K = -9.31 - -13.0 of experiments conducted under similar pressure and temperature conditions with different fluids, solids and flow regime (Pokrovsky et al., 2005; Gautelier et al., 2007; Pokrovsky et al., 2009).

Table 3.3: Comparisons of previous work on the dissolution of carbonate minerals at elevated pCO_2 values. Bolded words indicate the most significant differences in other studies from this one. All studies cited used synthetic brines, and calculate dolomite dissolution rates based on K_{Mg}.

Study	Solids	Fluids	Physical conditions (P, T pH)	Experimental design notes.	Reported results Log K mol/cm^{2}s
Pokrovsky et al., 2009	Dolomite, Magnesite, Calcite	0.1M NaCl	25-150 °C, 1-55 bar pCO_2, pH 3-6	Closed system and **mixed flow** in stirred reactors, Flame AA, ~700 minute experiments	-9.31 – -10.21
Pokrovsky et al. 2005	Dolomite, Calcite	0.001-0.1M NaCl	**25 °C**, 0-50 bar pCO_2	Powders, and rotating disk in both Closed system and **mixed flow** in stirred reactors, Flame AA, ~700 minute experiments	-11.7 - -10.8
Gautelier et al., 2007	Dolomite	HCl-$NaHCO_3$	80 °C, pH: 6.36-7.17	**Mixed Flow**, Flame AA,	-11.6 – -13.0
Saldi et al., 2010	**Magnesite**	0.001-1M	**150-200 °C**,	Batch and **mixed flow**, Flame AA	-9.9- -11.6
Heeschen et al., 2010	Dolomite	150-350 g/l	**< 590 bar, < 350 °C**	Unstirred batch reactor, ICP-OES, ICP-MS	~2% dissolution
This Study	Dolomite (minor Calcite)	0.3-0.4M	105 °C, 50 bar	Agitated batch reactor, ICPMS, IC	-9.80 - -10.12

Carbonates will vary a great deal based on mode of formation and diagenetic history. These differences will express themselves through a range of dissolution rates dependent upon factors such as grain morphology, composition, and surface impurities. Natural carbonates display orders of magnitude higher concentrations of impurities on their surfaces than do synthetic or pristine samples, which leads to greater dissolution rates of synthetic carbonates (Herman and White, 1985; Eisenlohr et al., 1999).

Experimental design has also been shown to play an integral role in influencing reaction rates. Reactor dimensions, stirring rates, measurement methods, and water rock ratios have all been demonstrated to effect carbonate dissolution rates (Sjoberg and Rickard, 1983). In an effort to reduce the thickness of the boundary layer "d" (Figure 3.2), a rotating disk apparatus is utilized (Sjoberg and Rickard, 1983); both the disk rotation speed and stirring rate within reactors have been shown to enhance dissolution kinetics (Pokrovsky et al., 2009). The size of grains used in experiments also has proven to influence rates of dissolution. Observational studies of calcite that measure reaction rates based on measurements from images of the changes in size of individual carbonate grains have shown that decreases in grain size lead to higher kink and step density –the primary sites of dissolution (Arvidson et al., 2003). Finally it has been noted that there is a discrepancy between powder experiments, and observational experiments with observational experiments having dissolution rates up to two orders of magnitude less than powder experiments (Morse and Arvidson, 2002; Morse et al., 2007).

3.4.4 Synthetic versus Real Brine

To explore the role of brine chemistry on dissolution rates, synthetic brines were constructed using natural Keg River brine major ion chemistry as a template, which included amounts of Na^+, K^+, Mg^{2+}, Ca^{2+}, SO_4^{2-}, HCO_3^- and Cl^-. The dissolution rates determined in these experiments yielded increased reaction rates tracked through releases in both Ca^{2+} and Mg^{2+}. The rate of release of Ca^{2+} was approximately 12% higher for the synthetic brine than that of natural brines with rates of Log K_{Ca} = -9.24 ±0.21 and -9.29 ±0.04 respectively. In the case of Mg^{2+} the increase in reaction rate for synthetic brines was more pronounced with rates of Log K_{Mg} of -9.81 ±0.02 and -9.46 ±0.09 respectively,

over a 120% increase. These results indicate that in addition to salinity and major bulk ion chemistry in solution, trace element chemistry plays a significant role in dissolution rates of dolomite, particularly around the >MgOH reactive site.

Evaluating the impact that trace element interactions exert on reaction rates of carbonate rocks is a very complex task, and there are numerous studies which have made progress in quantifying certain geochemical processes over a specific pressure, temperature, salinity and pH range. The majority of these processes have yet to be incorporated into geochemical models applied to the response of formations to CO_2 injection. Individual species can dramatically influence not only the rate of dissolution but also the dissolution process at the mineral-fluid interface (Morse and Berner, 1972; Thomas et al., 1993; Lea et al., 2001; Pokrovsky and Schott, 2002; Vinson and Luttge, 2005; Arvidson et al., 2006; Ruiz-Agudo et al., 2009; Ruiz-Agudo et al., 2011). For example light alkali metals in solution will destabilize the hydration shells around ions, rendering the solvent less effective in dissolving dolomite (Ruiz-Agudo et al., 2011). In addition the presence of Mn^{2+} in solution, inhibits dissolution on carbonate surfaces (Arvidson et al., 2003). Quantifying the contributions of individual ions to either the catalysis or inhibition of dissolution rates has started, however extrapolating these results to the full range of possible conditions – relevant to CCS – is still lacking.

3.4.5 The Effect of Zn^{2+} and Sr^{2+} on Rate Constants

To contribute to the growing body of knowledge characterizing CO_2 storage in reservoir fluids, the effects of Zn^{2+} and Sr^{2+} in solution on rate constants were investigated. Experiments were conducted at 50 bar pCO_2 and 105 °C with Keg River carbonates in the presence of synthetic brines spiked with either $SrCl_2$ or $ZnCl_2$ to

investigate the influence of these two ions, which are present in Keg River brine at notable concentrations (Table 3.1). Fluid spiked with $ZnCl_2$ yield rate constants of -9.30 ±0.21 and -9.67 ±0.09 for Log K_{Ca} and Log K_{Mg} respectively; fluid spiked with $SrCl_2$ yield rate constants of -9.15 ±0.21 and -9.43 ±0.09 for Log K_{Ca} and Log K_{Mg} respectively.

Compared to the original synthetic brine, the spiked solution containing Zn^{2+} showed nearly an identical K_{Ca} value, however the value of K_{Mg} displayed a reduction by over nearly 40%. A similar trend was found for the spiked solution containing Sr^{2+} for K_{Ca}, which showed a 20% increase, however K_{Mg} was within 10% of the original synthetic brine. The behaviour of Sr^{2+} corroborates previous studies based on observational studies on calcite grains, in that the presence of Sr^{2+} does not exert a significant change in rate constants (Lea et al., 2001; Vinson and Luttge, 2005). The effect of Zn^{2+} on K_{Mg} suggests that the presence of this ion inhibits hydration of the MgOH site on dolomite surfaces. This effect has been shown in studies involving calcite growth (Glasner and Weiss, 1980; Temmam et al., 2000; Freij et al., 2005)(Freij et al., 2005), however this is the first time this phenomena has been reported in Mg-bearing carbonates at reservoir conditions.

3.5 Applications

Reactive transport models combine geochemical proxies such as local equilibrium and kinetic data with mass transport models commonly utilized for hydrogeology and reservoir simulations (Bethke, 2008). When provided with accurate field data, reactive transport models are the best geochemical forecasting method available today. By combining information about where and when reactions occur to the physical properties of a reservoir and its flow regime, this tool can be very powerful in predicting the

physical and geochemical impacts, and distribution between storage mechanisms over the lifetime of a CCS projects. It is impossible to encapsulate the full complexity of natural systems, however progress has been made in identifying important processes that play a significant role in the evolution of injected CO_2 into the subsurface. Upscaling reaction rate constants developed from laboratory scale experiments to heterogeneous porous media where reactions will occur in natural systems is underway (Li, et al., 2006). Another constraint on the application of reactive transport models is the behaviour of CO_2 upon injection. Recent work has introduced convective flow of dense CO_2-fluid with aquifer brine (Nordbotten et al., 2005; Xu et al., 2006) and fingering of CO_2 into the brine (Nordbotten et al., 2005).

In order for reactive transport simulations to be accurate, there must be high quality and relevant data input into them. Expanding current databases to include rate constants measured at or near reservoir conditions on materials, which reflect the full gamut of materials in potential CO_2 storage reservoirs, is essential in achieving this task. The work conducted here was performed in this spirit to provide the most accurate laboratory data possible, specific to the Fort Nelson CCS project.

3.6 Summary

This study presented new data measured for the dissolution rates of the Keg River formation at 105 °C and 50 bar pCO_2 immersed into natural and synthetic brine. This data will help to predict the impacts of injecting millions of tons of CO_2 into the Keg River formation, and has the potential to perform a direct comparison of laboratory measured reaction rates with field observations, which most dissolution studies are not able to do. Results found significant increases in K_{Mg} and moderate increases in K_{Ca} for

synthetic brines compared to natural Keg River waters. These results are significant because the majority of previous work has only used synthetic brines to measure rate constants, which if applied to a natural system such as a CO_2 storage project, may overestimate reaction rates by over two factors. To explore this discrepancy, two trace ions present in natural Keg River waters, Sr^{2+}, and Zn^{2+} were added to synthetic solutions at 10 mmol concentrations, in order to explore the influence of minor constituents. Solutions spiked with Zn^{2+} were found to have a significant reduction in K_{Mg} and no effect on K_{Ca}, however solutions spiked with Sr^{2+} showed a slight increase in K_{Ca} and virtually no change in K_{Mg}.

Using synthetic brines in experiments as proxies for natural systems may lead to large over estimates of rate constants, as was demonstrated in this study producing rate constants for the >MgOH hydration site over two factors lower than natural waters. This study articulates the importance of trace elements on dissolution rates along with pCO_2, temperature, and salinity –parameters that dominate the literature.

3.7 Future Work

Expanding the current set of experiments to further trials over a broader set of pressure, temperature and salinity conditions would allow the calculation of activation energies from the Arrhennius equation, and a greater understanding of the physical constraints on CO_2 injection. While this information would not present a direct benefit to the Fort Nelson CCS project, it would provide a more comprehensive data set for the future proliferation of this technology.

Currently there are two fundamental problems within the literature. First, there are inconsistencies with observational measurements of mineral surfaces where reaction rates

are calculated from images of etch pit formation and kink propagation, and geochemical experiments similar to those conducted in this work. Observational work where dissolution rates are measured from SEM images through changes in rock grain dimensions, was attempted unsuccessfully; however future work utilizing known methods found in the literature involving Atomic Force Microscopy or Field Emission Scanning Electron Microscopy may shed light on this short-coming in experimental geochemistry. Second, a standardization of carbonate dissolution experiments at specific pressures, temperatures, salinities, brine chemistries, solids, and fluid rock ratios, would allow more direct comparisons of different studies. This would potentially allow for the quantification of how experimental design can impact reaction rates.

Finally, work conducted here on trace element interactions on dissolution kinetics must be expanded to produce more comprehensive geochemical models with the capacity to replicate natural systems. More batch reactor experiments with ICPMS measurements of different brines spiked with the full suite of elements found in natural waters over varying concentrations would cover significant ground in achieving this goal.

Chapter 4: Research Summary and Conclusions

If the world is going to collectively mitigate the problem of climate change through large reductions in CO_2 emissions, solutions are needed which can be deployed at the front end of this century. CCS is one potential technology, which may be a significant part of this effort. CCS has the benefits of capitalizing on a large existing workforce, and experience in transport and storing large quantities of gaseous species. If this technology is going to fulfill its projected potential, a combination of research and development and learning by doing needs to occur to improve on both reducing, and quantifying the risks associated with CCS, and making large efficiency gains. The best way to achieve these goals is through pilot and full-scale demonstration projects where predictions made in the laboratory can be tested in a real world setting.

The Fort Nelson CCS project has the potential to be a world-class demonstration of this technology. CCS in the context of fossil fuel extraction, processing and refining represents approximately 4% of global CO_2 emissions (World Resource Institute, 2005). The Fort Nelson CCS project has the benefit of having low costs in gas separation, and it is inline with CO_2 reduction targets set by the British Columbia provincial government. If this project is deployed it will be a real example of CO_2 storage in a carbonate hosted saline aquifer, which will likely be one of the most dominant types of storage reservoirs.

The Keg River Formation was determined to have a large potential for CO_2 storage based on the results from this work. The Keg River formation is at a depth where pressure and temperature conditions are amenable to storing CO_2 in a dense supercritical state. Furthermore the hydrothermal dolomite reservoir rock will have relatively low reactivity as a carbonate reservoir, which will help to reduce sediment compaction. The

brine chemistry of the Keg River formation was also found to possess attractive attributes for the purposes of CO_2 storage in that measurements conducted in this work suggests that not only is the Keg River formation isolated from above formations, but it is also relatively fresh which will allow for more CO_2 to be trapped via solubility trapping which has been identified as the dominant trapping mechanism over the 1000-1000000 year range.

The second part of this work looked at the response of reservoir rocks to changes in brine chemistry that injected CO_2 exerts on the system. The motivation behind this was to generate rate constants from the actual rocks that will be experiencing these changes for the Fort Nelson CCS Project. Results showed that upon CO_2 injection the pH of the reservoir brine abruptly dropped (Figure 3.8). This moved the solids in the system from a saturated to undersaturated state, which promoted dissolution. Powder experiments within a batch reactor determined that under reservoir temperatures of 105 °C and a pressure of 50 bar pCO_2 that the Keg River formation rocks will dissolve at an average rate of Log K_{Mg} = -9.80 ±0.02 mol·cm^{-2}·s^{-1}.

Rate constants derived in this work would be most effective if incorporated into a full reactive transport simulation. Once coupled to a hydrodynamic flow model this geochemical data would help to determine when, where, and the magnitude chemical reactions are occurring in the Keg River formation. Some examples of topics this study will contribute to include: the amount of global dissolution and increase in porosity in a reservoir, the competency of rock near the injection center, and changes in reservoir brine chemistry. Without this new data geochemical predictions for the Keg River formation would be based on experiments using synthetic brines, which this study demonstrated will

over-estimate dissolution rates. The importance of this information in the long-term viability of a CCS project is that it helps to predict the distribution of CO_2 between different trapping mechanisms over time. This is important in the short, and long-term risk assessment studies of CCS projects.

The current state of models that predict the behaviour of formations undergoing CO_2 injection is that they are constantly evolving better mathematical code to incorporate the physical characteristics of CO_2 injection, but are still completely reliant on the data incorporated into them. Most laboratory analysis of the dissolution rates of carbonates is performed at pCO_2 values less than or equal to 1 bar. Of the studies that do experiment at high pCO_2 values, the geochemistry and hydrodynamic conditions are tightly controlled. These simplifications often lead to overestimations of reaction rates and fail to capture the complexity of natural systems. This work found that when comparing natural to synthetic brines, there is an increase in dissolution rates by over 120%. This was attributed to trace ion chemistry, which later experiments supported when solutions spiked with Sr^{2+} and Zn^{2+} were found to have K_{Mg} values of -9.43 ±0.09, and -9.67 ±0.09 respectively, demonstrating the strong influence that individual species can exert on dissolution rates.

In summary this work evaluated a potential CCS project on geochemical criteria, and then performed experiments to provide key information for the response of a formation to injected CO_2. What is unique about this work is that it uses rocks and fluids actually from a potential CCS project, which means that predictions of this work can be tested in a full-scale CCS project.

If we make the assumption that developing economies will follow in the footsteps of industrialized ones and will not resist the temptation of cheap power and rapid industrialization, than CCS will need to be an integral part of the effort to reduce global

GHG emissions in the 21st century. If CCS is to reach the level of full deployment, than gas processing facilities such as the Fort Nelson project will need to be part of the demonstration phase for this technology to prove the viability of CCS in the near future.

Bibliography

Al-Aasm, I., 2003. Origin and characterization of hydrothermal dolomite in the Western Canada Sedimentary Basin. *Journal of Geochemical Exploration* **78**, 9-15.

Allen, D., Strazisar, B., Soong, Y., and Hedges, S., 2005. Modeling carbon dioxide sequestration in saline aquifers: Significance of elevated pressures and salinities. *Fuel processing technology* **86**, 1569-1580.

Arvidson, R. S., Collier, M., Davis, K. J., Vinson, M. D., Amonette, J. E., and Luttge, A., 2006. Magnesium inhibition of calcite dissolution kinetics. *Geochimica et cosmochimica acta* **70**, 583-594.

Arvidson, R. S., Ertan, I. E., Amonette, J. E., and Luttge, A., 2003. Variation in calcite dissolution rates: A fundamental problem? *Geochimica et cosmochimica acta* **67**, 1623-1634.

Arvidson, R. S. and Luttge, A., 2009. Mineral dissolution kinetics as a function of distance from equilibrium-New experimental results. *Chemical geology* **269**, 79-88.

Aulstead, K. and Spencer, R., 1985. Diagenesis of the Keg River Formation, northwestern Alberta: fluid inclusion evidence. *Bulletin of Canadian Petroleum Geology* **33**, 167.

Bachu, S., 2006. The Potential for Geological Storage of Carbon Dioxide in Northeastern British Columbia. *British Columbia Resource Developement and Geoscience Branch Summary of Activities 2006*.

Bachu, S., Bonijoly, D., Bradshaw, J., Burruss, R., Holloway, S., Christensen, N. P., and Mathiassen, O. M., 2007. CO2 storage capacity estimation: Methodology and gaps. *International Journal of Greenhouse Gas Control* **1**, 430-443.

Bachu, S., 2008. CO2 storage in geological media: Role, means, status and barriers to deployment. *Progress in Energy and Combustion Science* **34**, 254-273.

Bachu, S. and Burwash, R., 1994. Geothermal regime in the Western Canada sedimentary basin. *GD Mossop and I. Shetsen, comp., Geological Atlas of the Western Canada sedimentary basin: Calgary, Canadian Society of Petroleum Geologists and Alberta Research Council*, 447-454.

Baumert, K. A., Herzog, T., and Pershing, J., 2005. *Navigating the numbers: Greenhouse gas data and international climate policy*. The World Resources Institute, 10 G Street, NE Suite 800 Washington, D. C. 20002 USA.

Bentley, R. W., 2002. Global oil & gas depletion: an overview. *Energy Policy* **30**, 189-205.

Bethke, C., 2008. *Geochemical and biogeochemical reaction modeling*. Cambridge University Press.

Billings, G. K., Hitchon, B., and Shaw, D., 1969. Geochemistry and origin of formation waters in the western Canada sedimentary basin, 2. Alkali metals. *Chemical geology* **4**, 211-223.

Boulton, G., Caban, P., Van Gijssel, K., Leijnse, A., Punkari, M., and Van Weert, F., 1996. The impact of glaciation on the groundwater regime of Northwest Europe. *Global and Planetary Change* **12**, 397-413.

Brunauer, S., Emmett, P. H., and Teller, E., 1938. Adsorption of gases in multimolecular layers. *Journal of the American Chemical Society* **60**, 309-319.

Connolly, C. A., Walter, L. M., Baadsgaard, H., and Longstaffe, F. J., 1990. Origin and evolution of formation waters, Alberta Basin, Western Canada Sedimentary Basin. II. Isotope systematics and water mixing. *Applied Geochemistry* **5**, 397-413.

Crockford, P. and Telmer, K., 2010 Exploring the Fate of CO_2 at British Columbia's Planned Fort Nelson Carbon Capture and Storage Project. Geoscience Reports 2009, *BC Ministry of Energy, Mines and Petroleum Resources,* pages 1–4.

Davies, G. R. and Smith Jr, L. B., 2006. Structurally controlled hydrothermal dolomite reservoir facies: An overview. *AAPG bulletin* **90**, 1641.

Duan, Z. and Sun, R., 2003. An improved model calculating CO2 solubility in pure water and aqueous NaCl solutions from 273 to 533 K and from 0 to 2000 bar. *Chemical geology* **193**, 257-271.

Dunsmore, H.E. 1971. Diagenetic Model for the Middle Devonian Keg River Formation, Rainbow Area, Northwestern Alberta. Unpublished **M.Sc**. **thesis**

Eccles, J. K., Pratson, L., Newell, R. G., and Jackson, R. B., 2009. Physical and economic potential of geological CO2 storage in saline aquifers. *Environmental science & technology* **43**, 1962-1969.

Eisenlohr, L., Meteva, K., Gabrovek, F., and Dreybrodt, W., 1999. The inhibiting action of intrinsic impurities in natural calcium carbonate minerals to their dissolution kinetics in aqueous H2O-CO2 solutions. *Geochimica et cosmochimica acta* **63**, 989-1001.

Ellis, A., 1959. The solubility of calcite in carbon dioxide solutions. *American Journal of Science* **257**, 354.

Finneran, D. W. and Morse, J. W., 2009. Calcite dissolution kinetics in saline waters.

Chemical geology **268**, 137-146.

Fischer, C. and Gaupp, R., 2004. Multi-scale rock surface area quantification--a systematic method to evaluate the reactive surface area of rocks. *Chemie der Erde-Geochemistry* **64**, 241-256.

Freij, S. J., Godelitsas, A., and Putnis, A., 2005. Crystal growth and dissolution processes at the calcite-water interface in the presence of zinc ions. *Journal of Crystal Growth* **273**, 535-545.

Ganor, J. and Lasaga, A. C., 1998. Simple mechanistic models for inhibition of a dissolution reaction. *Geochimica et cosmochimica acta* **62**, 1295-1306.

Garrett, T. J., 2011. Are there basic physical constraints on future anthropogenic emissions of carbon dioxide? *Climatic Change*, 1-19.

Ghaderi, S. M., Keith, D. W., Lavoie, R., and Leonenko, Y., 2011. Risk associated with H2S evolution in sour aquifers during CO2 injection. *Energy Procedia* **4**, 4117-4123.

IEAGHG, I., 2006. CO2 capture as a factor in power station investment decisions. *IEA GHG (IEA Greenhouse Gas R&D Programme) Report*.

Gibbins, J. and Chalmers, H., 2008. Carbon capture and storage. *Energy Policy* **36**, 4317-4322.

Gilfillan, S. M. V., Lollar, B. S., Holland, G., Blagburn, D., Stevens, S., Schoell, M., Cassidy, M., Ding, Z., Zhou, Z., and Lacrampe-Couloume, G., 2009. Solubility trapping in formation water as dominant CO2 sink in natural gas fields. *Nature* **458**, 614-618.

Glasner, A. and Weiss, D., 1980. The crystallization of calcite from aqueous solutions and the role of zinc and magnesium ions--I. Precipitation of calcite in the presence of Zn2+ ions. *Journal of Inorganic and Nuclear Chemistry* **42**, 655-663.

Gledhill, D. K. and Morse, J. W., 2006. Calcite dissolution kinetics in Na-Ca-Mg-Cl brines. *Geochimica et cosmochimica acta* **70**, 5802-5813.

Grasby, S. E. and Chen, Z., 2005. Subglacial recharge into the Western Canada Sedimentary Basin--Impact of Pleistocene glaciation on basin hydrodynamics. *Bulletin of the Geological Society of America* **117**, 500.

Griffin, D., 1967. Devonian of northeastern British Columbia.

Hartling , A., 2008. Carbon Capture and Storage in British Columbia. Geoscience Reports 2008, *BC Ministry of Energy, Mines and Petroleum Resources,* pages 1–4.

Herman, J. S. and White, W. B., 1985. Dissolution kinetics of dolomite: Effects of lithology and fluid flow velocity. *Geochimica et cosmochimica acta* **49**, 2017-2026.

Hitchon, B., Billings, G. K., and Klovan, J., 1971. Geochemistry and origin of formation waters in the western Canada sedimentary basin--III. Factors controlling chemical composition. *Geochimica et cosmochimica acta* **35**, 567-598.

Hitchon, B. and Friedman, I., 1969. Geochemistry and origin of formation waters in the western Canada sedimentary basin--I. Stable isotopes of hydrogen and oxygen. *Geochimica et cosmochimica acta* **33**, 1321-1349.

Holubnyak, Y. I., Hawthorne, S. B., Mibeck, B. A. F., Miller, D. J., Bremer, J. M., Sorensen, J. A., Steadman, E. N., and Harju, J. A., 2011. Modeling CO2-H2S-water-rock interactions at Williston Basin reservoir conditions. *Energy Procedia* **4**, 3911-3918.

Kaszuba, J.P., Janecky, D.R., and Snow, M.G., 2003. Carbon dioxide reaction processes in a model brine aquifer at 200 C and 200 bars: implications for geologic sequestration of carbon. *Applied Geochemistry* **18** 1065-1080

Knauss, K. G., Johnson, J. W., and Steefel, C. I., 2005. Evaluation of the impact of CO2, co-contaminant gas, aqueous fluid and reservoir rock interactions on the geologic sequestration of CO2. *Chemical geology* **217**, 339-350.

Lea, A. S., Amonette, J. E., Baer, D. R., Liang, Y., and Colton, N. G., 2001. Microscopic effects of carbonate, manganese, and strontium ions on calcite dissolution. *Geochimica et cosmochimica acta* **65**, 369-379.

Li, L., Peters, C. A., and Celia, M. A., 2006. Upscaling geochemical reaction rates using pore-scale network modeling. *Advances in water resources* **29**, 1351-1370.

Li, L., Peters, C. A., and Celia, M. A., 2006. Reply to'Comments on upscaling geochemical reaction rates usingpore-scale network modeling'by Peter C. Lichtner and Qinjun Kang. *Advances in water resources* **43**.

Liteanu, E. and Spiers, C. J., 2009. Influence of pore fluid salt content on compaction creep of calcite aggregates in the presence of supercritical CO2. *Chemical geology* **265**, 134-147.

Liu, Z. and Wolfgang, D., 2001. Kinetics and rate-limiting mechanisms of dolomite dissolution at various CO 2 partial pressures. *Science in China Series B: Chemistry* **44**, 500-509.

Liu, Z., Yuan, D., and Dreybrodt, W., 2005. Comparative study of dissolution rate-determining mechanisms of limestone and dolomite. *Environmental Geology* **49**, 274-279.

Lumsden, D. N., and Lloyd, R. V., 2008. Three Dolomites. *Journal of Sedimentary Research.* **67**, 391-396

Machel, H. G., Krouse, H. R., and Sassen, R., 1995. Products and distinguishing criteria of bacterial and thermochemical sulfate reduction. *Applied Geochemistry* **10**, 373-389.

Machel, H. G. and Lonnee, J., 2002. Hydrothermal dolomite--a product of poor definition and imagination. *Sedimentary Geology* **152**, 163-171.

Mathias, S. A., Hardisty, P. E., Trudell, M. R., Zimmerman, R. W., 2009. Screening and selection of sites for CO2 sequestration based on pressure buildup. *International Journal of Greenhouse Gas Control* **3**, 577-585.

Mauna-Loa-Observatory, 2011. *NOAA-ESRL*.

McCamis, J. G. and Griffith, L. S., 1967. Middle Devonian facies relationships, Zama area, Alberta. *Bulletin of Canadian Petroleum Geology* **15**, 434.

Michael, K., Bachu, S., Buschkuehle, B., Haug, K., Grobe, M., and Lytviak, A., 2006. Comprehensive characterization of a potential site for CO2 geological storage in central Alberta, Canada.

Michael, K., Golab, A., Shulakova, V., Ennis-King, J., Allinson, G., Sharma, S., and Aiken, T., 2010. Geological storage of CO2 in saline aquifers--A review of the experience from existing storage operations. *International Journal of Greenhouse Gas Control* **4**, 659-667.

Mohr, S. and Evans, G., 2009. Forecasting coal production until 2100. *Fuel* **88**, 2059-2067.

Morrow, D. W., Stasiuk, L. D., and Zhao, M., 2001. Dolomitization and Burial Diagenesis of Devonian Slave Point and Keg River Formations in the Cordova Embayment Region of Northeast British Columbia, Canada.

Morse, J. W. and Arvidson, R. S., 2002. The dissolution kinetics of major sedimentary carbonate minerals. *Earth-Science Reviews* **58**, 51-84.

Morse, J. W., Arvidson, R. S., and L¸ttge, A., 2007. Calcium carbonate formation and dissolution. *Chemical reviews* **107**, 342-381.

Morse, J. W. and Berner, R. A., 1972. Dissolution kinetics of calcium carbonate in sea water: II. A kinetic origin for the lysocline. *American Journal of Science.* **22,** 840-851

Morse, J. W. and Mackenzie, F. T., 1990. *Geochemistry of sedimentary carbonates*. Elsevier Science.

Nelson, S. J., 1970. *The Face of Time, the Geological History of Western Canada.* pp. 56-67 Alta. Soc. Petrol. Geol.

Nordbotten, J. M., Celia, M. A., and Bachu, S., 2005. Injection and storage of CO 2 in deep saline aquifers: Analytical solution for CO 2 plume evolution during injection. *Transport in Porous Media* **58**, 339-360.

Pacala, S. and Socolow, R., 2004. Stabilization wedges: solving the climate problem for the next 50 years with current technologies. *Science* **305**, 968.

Paquette, J. and Reeder, R. J., 1995. Relationship between surface structure, growth mechanism, and trace element incorporation in calcite. *Geochimica et cosmochimica acta* **59**, 735-749.

Parry, M. L., 2007. *Climate Change 2007: impacts, adaptation and vulnerability: contribution of Working Group II to the fourth assessment report of the Intergovernmental Panel on Climate Change*. Cambridge Univ Pr.

Patz, J. A., Campbell-Lendrum, D., Holloway, T., and Foley, J. A., 2005. Impact of regional climate change on human health. *Nature* **438**, 310-317.

Patzek, T. W., 2010. Subsurface Sequestration of CO 2 in the US: Is it Money Best Spent? *Natural resources research* **19**, 1-9.

Plummer, L., Wigley, T., and Parkhurst, D., 1978. The Kinetics of Calcite Dissolution in C 02-Water Systems at 5 Deg to 60 Deg C and 0. 0 to 1. 0 ATM C 02. *American Journal of Science* **278**.

Pokrovsky, O. and Schott, J., 2002. Surface chemistry and dissolution kinetics of divalent metal carbonates. *Environmental science & technology* **36**, 426-432.

Pokrovsky, O. S., Golubev, S. V., and Schott, J., 2005. Dissolution kinetics of calcite, dolomite and magnesite at 25 C and 0 to 50 atm pCO2. *Chemical geology* **217**, 239-255.

Pokrovsky, O. S., Golubev, S. V., Schott, J., and Castillo, A., 2009. Calcite, dolomite and magnesite dissolution kinetics in aqueous solutions at acid to circumneutral pH, 25 to 150∞ C and 1 to 55 atm pCO2: New constraints on CO2 sequestration in sedimentary basins. *Chemical geology* **265**, 20-32.

Pokrovsky, O. S. and Schott, J., 2001. Kinetics and mechanism of dolomite dissolution in neutral to alkaline solutions revisited. *American Journal of Science* **301**, 597.

Pokrovsky, O. S., Schott, J., and Thomas, F., 1999. Processes at the magnesium-bearing carbonates/solution interface. I. A surface speciation model for magnesite. *Geochimica et cosmochimica acta* **63**, 863-880.

Porter, J. W., Price, R. A. and McCrossan R. G., 1982, The Western Canada Sedimentary Basin. *Roy Soc. Phil Trans.* **305**, 169-192.

Prigiobbe, V., Heenchen, M., Werner, M., Baciocchi, R., and Mazzotti, M., 2009. Mineral

carbonation process for CO2 sequestration. *Energy Procedia* **1**, 4885-4890.

Rietveld, H.M., 1966 *Acta Chrystallographica* **21** A228 Section A

Ruiz-Agudo, E., Kowacz, M., Putnis, C., and Putnis, A., 2009. The role of background electrolytes on the kinetics and mechanism of calcite dissolution. *Geochimica et cosmochimica acta* **74**, 1256-1267.

Ruiz-Agudo, E., Urosevic, M., Putnis, C. V., Rodriguez-Navarro, C., Cardell, C., and Putnis, A., 2011. Ion-specific effects on the kinetics of mineral dissolution. *Chemical geology*.

Schott, J., Pokrovsky, O. S., and Oelkers, E. H., 2009. The link between mineral dissolution/precipitation kinetics and solution chemistry. *Reviews in mineralogy and geochemistry* **70**, 207.

Schrag, D., 2009. Making Carbon Capture and Storage Work. *Acting in Time on Energy Policy*, 39-55.

Shevalier, M., Nightingale, M., Mayer, B., and Hutcheon, I., 2011. TOUGHREACT modeling of the fate of CO2 injected into a H2S containing saline aquifer: The example of the Wabamum Area Sequestration Project (WASP). *Energy Procedia* **4**, 4403-4410.

Shukla, R., Ranjith, P., Haque, A., Choi, X., 2010 A review of studies on CO_2 sequestration and caprock integrity. *Fuel* **89** 2651-2664

Sjoberg, E. L. and Rickard, D., 1983. The influence of experimental design on the rate of calcite dissolution. *Geochimica et cosmochimica acta* **47**, 2281-2285.

Sjoberg, E. L. and Rickard, D. T., 1984. Temperature dependence of calcite dissolution kinetics between 1 and 62 C at pH 2.7 to 8.4 in aqueous solutions. *Geochimica et cosmochimica acta* **48**, 485-493.

Solomon, S., 2007. *Climate change 2007: the physical science basis*. Cambridge University Press.

Sorensen, J. A., Smith, S., Steadman, E., Harju, J., Moffatt, D., Laundry, A., 2010. The Fort Nelson Carbon Capture and Storage Feasibility Project - A Program for Large-Scale Geologic Storage of CO2 from a Natural Gas-Processing Plant In British Columbia, Canada. *Energy Procedia*.

Szramek, K., McIntosh, J. C., Williams, E. L., Kanduc, T., Ogrinc, N., and Walter, L. M., 2007. Relative weathering intensity of calcite versus dolomite in carbonate-bearing temperate zone watersheds: Carbonate geochemistry and fluxes from catchments within the St. Lawrence and Danube river basins. *Geochemistry Geophysics Geosystems* **8**, Q04002.

Taylor, R. S., Mathews, W. H., and Kupsch W. O., 1964, Tertiary. In *Geological History of Western Canada* (eds R.G., McCrossan and R. P. Glaister), 190-194. Alta. Soc. Petrol. Geol.

Temmam, M., Paquette, J., and Vali, H., 2000. Mn and Zn incorporation into calcite as a function of chloride aqueous concentration. *Geochimica et cosmochimica acta* **64**, 2417-2430.

Thomas, M. M., Clouse, J. A., and Longo, J. M., 1993. Adsorption of organic compounds on carbonate minerals:: 1. Model compounds and their influence on mineral wettability. *Chemical geology* **109**, 201-213.

Titiloye, J., De Leeuw, N., and Parker, S., 1998. Atomistic simulation of the differences between calcite and dolomite surfaces. *Geochimica et cosmochimica acta* **62**, 2637-2641.

Vinson, M. D. and Luttge, A., 2005. Multiple length-scale kinetics: An integrated study of calcite dissolution rates and strontium inhibition. *American Journal of Science* **305**, 119.

Vukalovich, M. P. and Altunin, V. V., 1968. Thermophysical Properties of Carbon Dioxide. *Thermophysical Properties of Carbon Dioxide.*

Xu, X., Chen, S., and Zhang, D., 2006. Convective stability analysis of the long-term storage of carbon dioxide in deep saline aquifers. *Advances in water resources* **29**, 397-407.

Yang, F., Bai, B., Tang, D., Shari, D. N., and David, W., 2010 Characteristics of CO2 sequestration in saline aquifers. *Petroleum Science* **7**, 83-92.

Appendices

Appendix I

XRD Diffractograms

This appendix presents results from XRD analysis at the University of British Columbia, for samples collected from the Keg River Formation in May 2009.

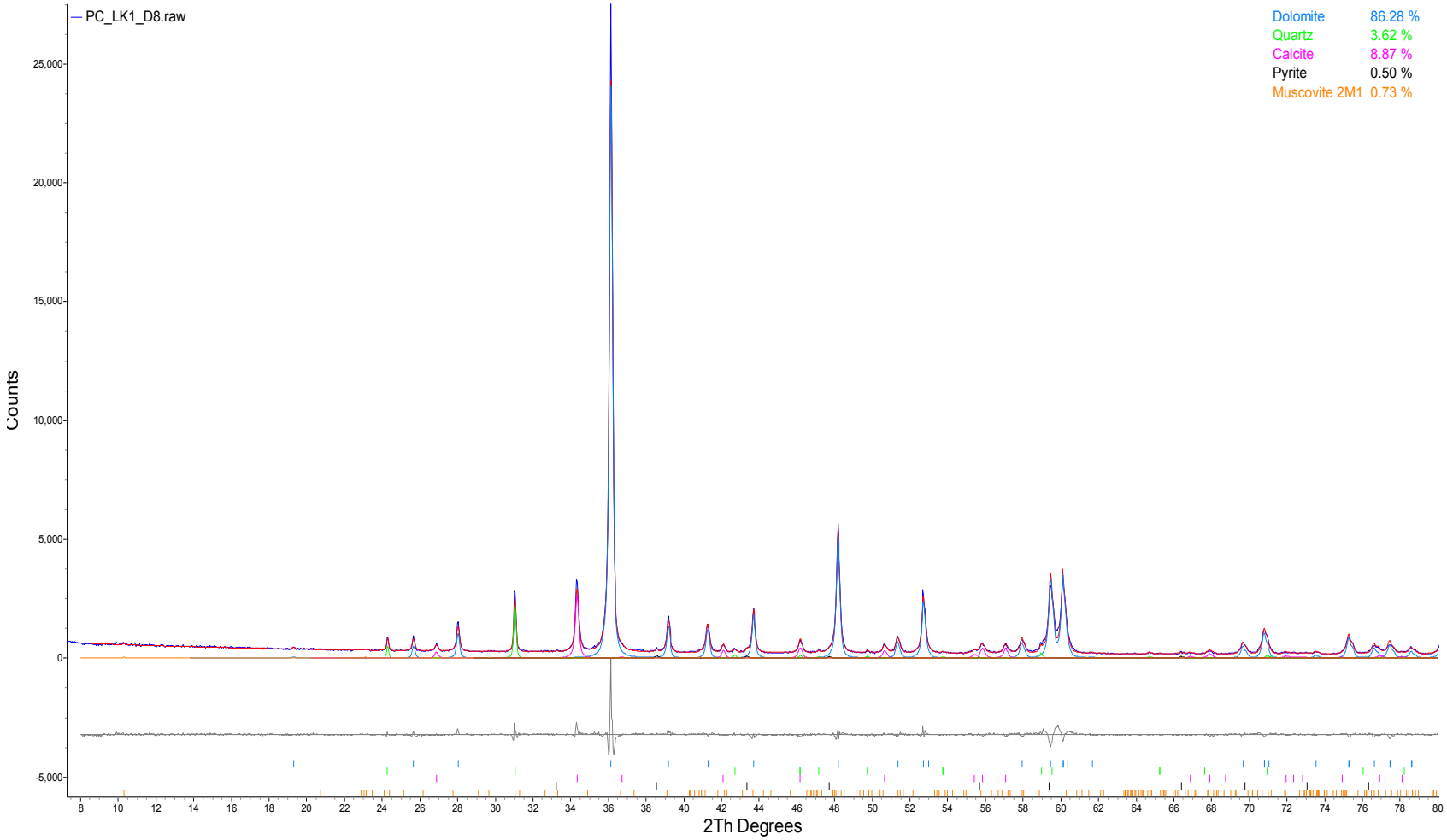

XRD diffractogram of sample **"LK-1"** (lower Keg River formation)(blue line - observed intensity at each step; red line - calculated pattern; solid grey line below – difference between observed and calculated intensities; vertical bars, positions of all Bragg

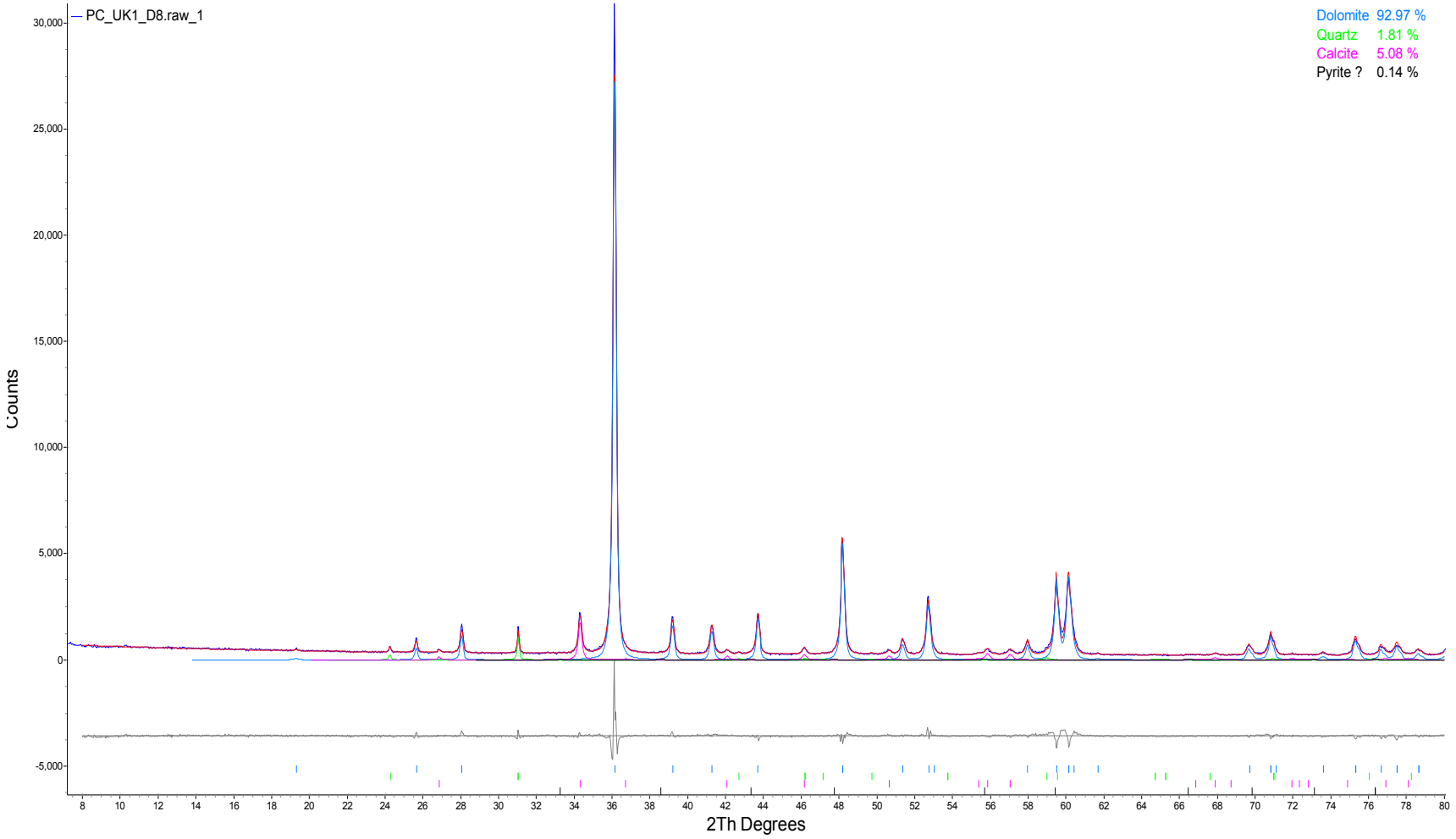

XRD diffractogram of sample **"UK-1"** (Upper Keg River Formation)(blue line - observed intensity at each step; red line - calculated pattern; solid grey line below – difference between observed and calculated intensities; vertical bars, positions of all Bragg reflections). Coloured lines are individual diffraction patterns of all phases.

Appendix II

Experimental Apparatus Homogeneity Test Results

This Appendix presents results from tests for homogeneity within the reactor used for experiments. During experiments the reactor was agitated every 30 min. Upon completion the reactor was opened and water was pipetted out at different depths, and was then analyzed for major ions. Ion concentrations are presented in mmol units.

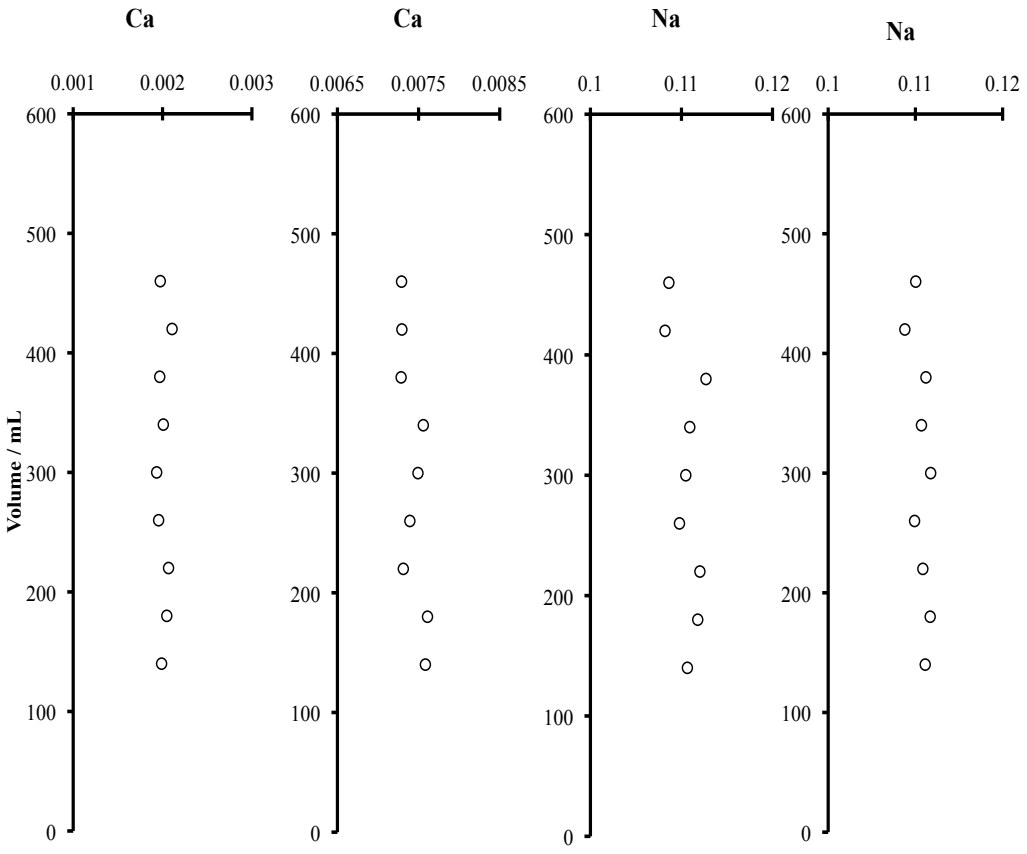

Appendix III

Surface Area Determination by Conductivity Measurements

This Appendix presents results from 40 experiments, which tried to quantify how much solid is actually reacting at any given time. This was achieved through experiments using synthetic brines, at 105 °C, 50 bar pCO_2. Reaction rate is given in units of micro-siemens per minute (uS/min) a standard unit for conductivity.

Trial	Rock Mass (g)	Fluid	Time (min)	Conductivity (uS)	Rate (uS/min)
1	0.4972	Syn	0	31000	4.90
			105	32790	
			205	33740	
			291	34060	
			495	34320	
			605	34470	
2	0.0096	Syn	0	31000	1.98
			89	30840	
			226	31280	
			303	31300	
			448	31470	
			508	32110	
3	0	Syn	0	31000	1.76
			120	31400	
			260	31780	
			377	31850	
			546	31980	
4	12.6358	Syn	0	31000	5.28
			110	31650	
			380	31850	

			600	34050	
			770	35200	
5	0.1086	Syn	0	31000	4.96
			120	31410	
			250	32170	
			370	32560	
			490	33480	
6	12.5013	Syn	0	31000	5.44
			100	33950	
			200	34700	
			400	33800	
			600	35600	
7	2.3632	Syn	0	31000	5.30
			98	33300	
			206	33600	
			390	34100	
			520	34600	
8	0.0507	Syn	0	31000	3.75
			135	31600	
			202	32400	
			360	32700	
			512	32900	
9	0.116	Syn	0	31870	5.03
			76	32600	
			206	33000	
			267	33920	
			378	34020	
			507	34430	

10	0.0294	Syn	0	31000	2.69
			85	31970	
			303	32450	
			418	32220	
11	0.0514	Syn	10	31000	3.04
			69	31560	
			217	32100	
			262	32130	
			378	32480	
			507	32590	
12	0.202	Syn	0	31000	4.75
			100	32480	
			274	33270	
			406	33640	
			533	33990	
			580	34100	
13	0.0431	Syn	0	31000	2.69
			94	31530	
			212	31950	
			345	32320	
			426	32420	
			543	32460	
14	12.5	Syn	0	31000	5.20
			100	32610	
			200	33420	
			300	33620	
			406	33890	
			521	34000	

15	12.4	Syn	0	31000	4.32
			87	32360	
			181	33020	
			343	33340	
			415	33510	
			539	33650	
16	12.6	Syn	0	31000	5.35
			110	32580	
			191	33640	
			306	34090	
			471	34220	
			554	34330	
17	12.55	Syn	0	31000	4.97
			100	32310	
			207	32740	
			295	32680	
			441	33880	
			506	33640	
18	0.0169	Syn	0	31000	2.05
			100	31640	
			200	31880	
			302	32050	
			409	32110	
			500	32130	
19	12.66	Syn	0	31000	5.21
			100	32740	
			193	33410	

			304	33920	
			439	34200	
			561	34190	
20	12.63	Syn	0	31000	5.10
			94	32860	
			201	33510	
			317	33820	
			452	34000	
			509	34100	
21	12.34981	Syn	0	31000	4.99
			100	32670	
			200	33320	
			302	33720	
			421	33760	
			483	33710	
22	12.5123	Syn	0	31000	4.89
			96	32790	
			192	33320	
			300	33860	
			418	34020	
			550	34020	
23	0.0347	Syn	0	31000	2.34
			121	31610	
			217	32010	
			303	32160	

			432	32220	
			504	32250	
24	0.0784	Syn	0	31000	4.2170
			101	32320	
			208	32670	
			296	33100	
			471	33620	
			607	33820	
25	1.651	Syn	0	31000	5.17
			84	32150	
			192	32680	
			203	32950	
			311	33620	
			428	33820	
			543	33940	
26	0.916735	Syn	0	31000	4.97
			84	32360	
			192	32750	
			287	33000	
			394	33620	
			507	33780	
27	0.92460981	Syn	0	31000	4.72
			100	32420	
			200	32740	
			300	32770	
			404	33560	

			498	33610	
28	0.1321908	Syn	0	31000	5.32
			100	32600	
			207	33520	
			299	33770	
			401	33860	
			515	34000	
29	6.7481	Syn	0	31000	5.08
			74	32700	
			186	33530	
			309	33770	
			398	33970	
			536	34160	
30	0.0800842	Syn	0	31000	4.43
			100	31990	
			200	32830	
			300	33310	
			400	33670	
			600	33660	
31	0.073891	Syn	0	31000	3.62
			100	32570	
			207	32830	
			312	33000	
			422	33120	
			535	33370	
32	0.500941	Syn	0	31000	5.31

			99	33170	
			202	33730	
			300	34200	
			408	34220	
			501	34020	
33	0.008	Natural	0	31000	1.33
			100	31480	
			200	31630	
			300	31700	
			400	31760	
			500	31740	
34	0.073257	Natural	0	31000	3.32
			88	31910	
			210	32420	
			300	32690	
			418	32870	
			500	32740	
35	1.46	Natural	0	31000	3.82
			85	31810	
			172	32430	
			298	32750	
			445	33170	
			532	33150	
36	0.10641	Natural	0	31000	3.86
			91	32310	
			188	32640	
			304	32940	
			402	33140	

			504	33230	
37	12.6	Natural	0	31000	3.79
			100	32430	
			156	32590	
			300	32950	
			398	33090	
			500	33270	
38	12.4	Natural	0	31000	4.20
			100	32610	
			200	32690	
			300	33070	
			400	33400	
			500	33390	
39	12.5	Natural	0	31000	3.62
			97	32310	
			201	32670	
			315	33010	
			405	32980	
			498	33070	
40	12.5	Natural	0	31000	4.04
			100	32300	
			200	32550	
			300	32990	
			400	32970	
			474	33210	

Appendix IV

Raw Data Table for Dissolution Experiments of Keg River Formation Rocks at 105 °C, 50 bar pCO2 in Natural and Synthetic Brines

This Appendix presents the raw data for dissolution experiments on rocks collected form the Keg River formation in Northeast British Columbia.

Exp. ID	Time (min)	Rock	Fluid	pH	[Ca] (mmol)	[Mg] (mmol)
DK-1	0	KR	KR	6.21	0.00	0.00
	100	KR	KR	6.17	0.22	0.19
	300	KR	KR	5.29	1.90	0.25
	500	KR	KR	5.33	3.55	0.34
	800	KR	KR	5.39	4.35	0.57
DK-2	0	KR	KR	6.27	0.00	0.00
	100	KR	KR	5.51	0.93	0.20
	300	KR	KR	5.39	3.16	0.33
	500	KR	KR	5.38	3.35	0.43
	800	KR	KR	5.46	4.05	0.45
DK-3	0	KR	KR	6.15	0.00	0.00
	100	KR	KR	5.44	0.88	0.16
	300	KR	KR	5.59	1.99	0.30
	500	KR	KR	5.57	3.29	0.41
	800	KR	KR	5.49	3.91	0.49
DK-4	0	KR	KR	6.46	0.00	0.00
	100	KR	KR	5.67	1.02	0.19
	300	KR	KR	5.76	2.34	0.28
	500	KR	KR	5.74	2.48	0.44

	800	KR	KR	5.81	3.26	0.49
DS-1	0	KR	Syn	6.82	0.00	0.00
	100	KR	Syn	6.1	0.35	0.00
	200	KR	Syn	5.71	1.52	0.16
	400	KR	Syn	5.74	1.47	0.21
	750	KR	Syn	5.89	1.80	0.12
DS-2	0	KR	Syn	6.41	0.00	0.00
	100	KR	Syn	5.33	0.92	0.74
	200	KR	Syn	5.41	0.55	1.07
	400	KR	Syn	5.39	2.92	1.23
	600	KR	Syn	5.52	3.24	1.56
	750	KR	Syn	5.47	4.09	1.77
DS-3	0	KR	Syn	6.43	0.00	0.00
	100	KR	Syn	5.51	1.75	0.91
	200	KR	Syn	5.5	1.17	1.11
	400	KR	Syn	5.72	5.24	1.65
	600	KR	Syn	5.63	5.59	1.77
	750	KR	Syn	5.52	6.69	1.89
DS-4	0	KR	Syn	6.46	0.00	0.00
	100	KR	Syn	5.78	2.64	0.86
	200	KR	Syn	5.51	2.07	1.19
	400	KR	Syn	5.43	4.92	1.56
	600	KR	Syn	5.48	5.21	1.77
	750	KR	Syn	5.64	6.51	1.97
DS-5	0	KR	Syn	6.31	0.00	0.00
	100	KR	Syn	5.28	1.82	0.82
	200	KR	Syn	5.41	1.72	1.15
	400	KR	Syn	5.37	5.07	1.40

	600	KR	Syn	5.59	5.86	1.85
	750	KR	Syn	5.46	6.41	1.93
DS-6	0	KR	Syn	6.4	0.00	0.00
	100	KR	Syn	5.61	0.77	0.70
	200	KR	Syn	5.47	0.50	1.07
	400	KR	Syn	5.55	2.94	1.36
	600	KR	Syn	5.62	4.29	1.60
	750	KR	Syn	5.49	5.74	1.89
DS-7	0	KR	Syn	6.63	0.00	0.00
	100	KR	Syn	5.4	1.20	0.70
	200	KR	Syn	5.28	1.07	1.11
	400	KR	Syn	5.39	3.89	1.23
	600	KR	Syn	5.33	4.19	1.56
	750	KR	Syn	5.36	6.01	1.69
DS-8	0	KR	Syn	6.41	0.00	0.00
	110	KR	Syn	5.53	0.47	0.37
	240	KR	Syn	5.6	0.00	0.58
	380	KR	Syn	5.71	3.14	1.23
	600	KR	Syn	5.58	4.22	1.60
	770	KR	Syn	5.56	5.51	1.89
DS-9	0	KR	Sr-Syn	6.52	0.00	0.00
	100	KR	Sr-Syn	5.47	0.47	0.28
	200	KR	Sr-Syn	5.38	0.77	0.43
	400	KR	Sr-Syn	5.33	2.59	0.58
	620	KR	Sr-Syn	5.48	6.21	0.74
	760	KR	Sr-Syn	5.37	7.78	0.87
DS-10	0	KR	Zn-Syn	6.28	0.00	0.00
	95	KR	Zn-Syn	5.63	1.70	0.62

	260	KR	Zn-Syn	5.66	2.35	1.19
	420	KR	Zn-Syn	5.61	4.59	1.51
	610	KR	Zn-Syn	5.58	6.09	1.87
	730	KR	Zn-Syn	5.63	6.39	2.11

Appendix V

Comparison of IC and ICPMS Results

This appendix presents results from both IC and ICPMS are compared for measurements of Ca in the same samples. Analysis was performed at the University of Victoria. Analytical error is within the size of the data points.

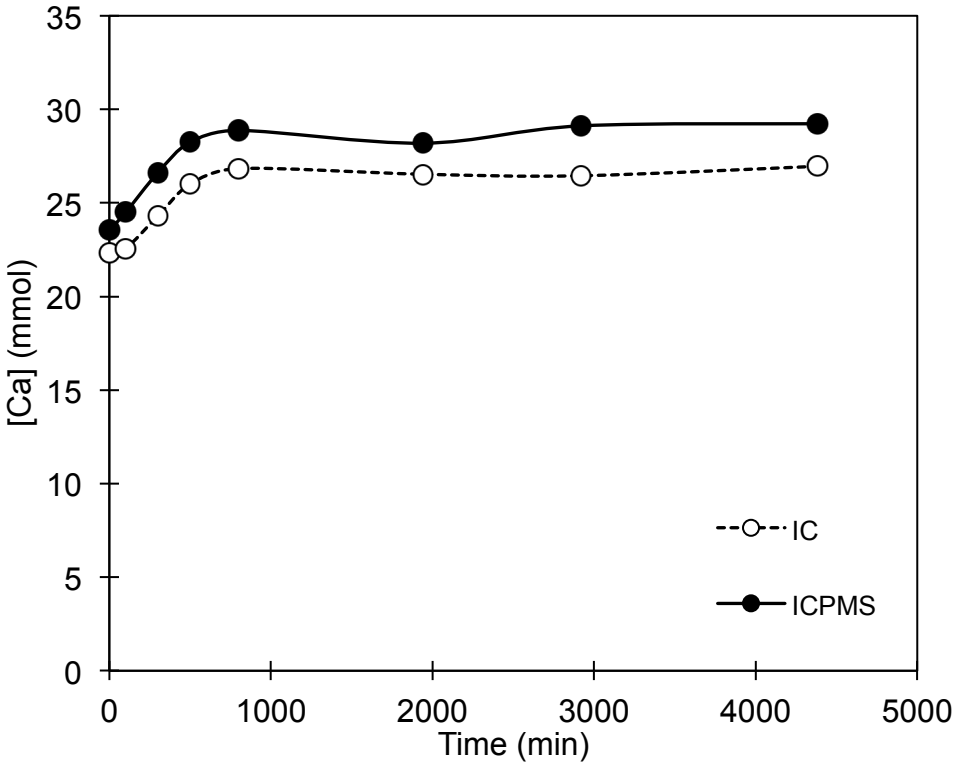

Appendix VI

Arrhenius Plots

This Appendix presents Arrhenius plots for experiments on Keg River Formation rock and fluid, at temperatures of 50, 105 and 200 °C, and 50 bar pCO_2. Results are presented with previous findings by Pokrovsky et al., (2009). Although Results differ the trends are found to be consistent where at temperatures greater than 100 °C there appears to be a negative activation energy.

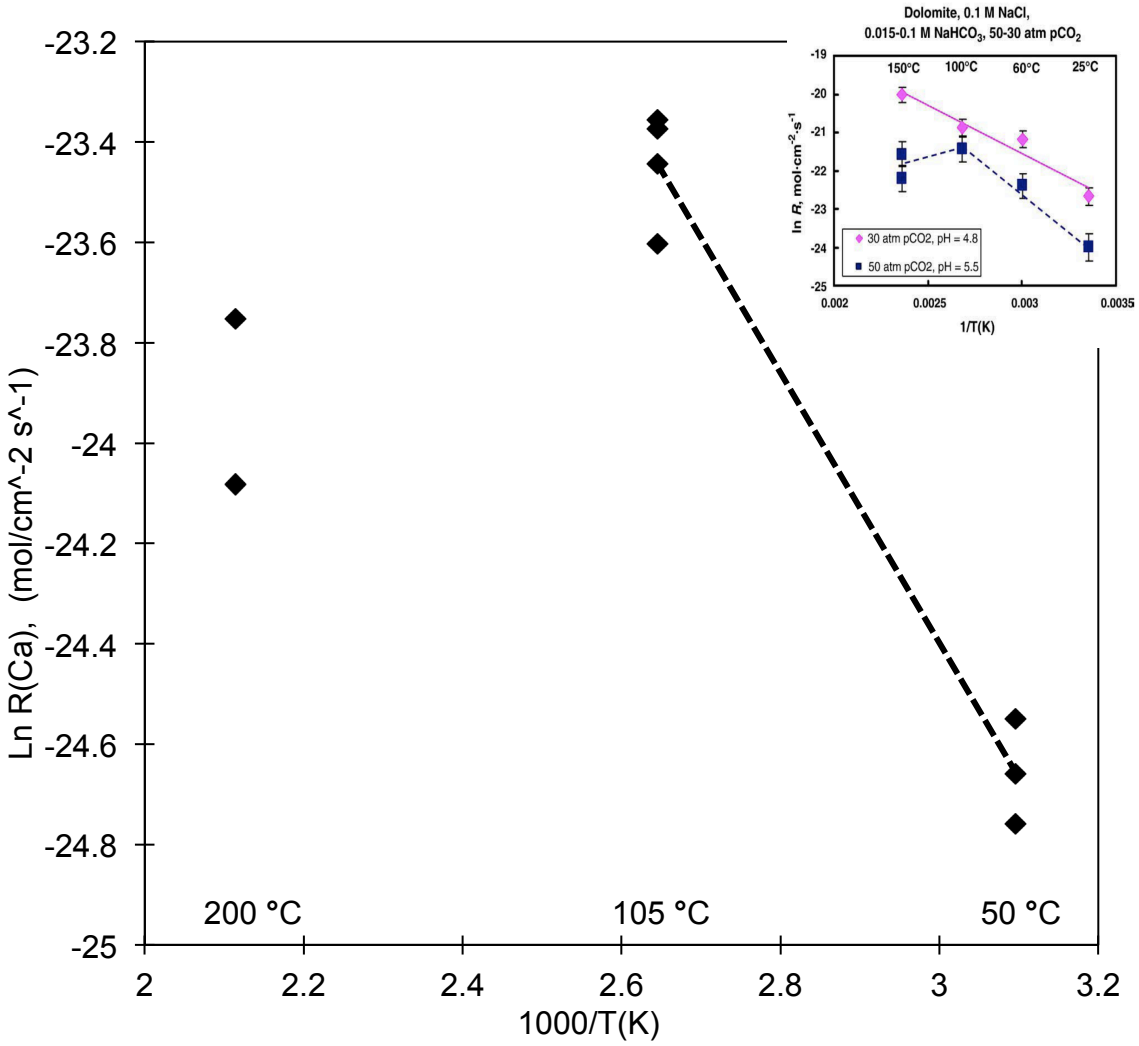

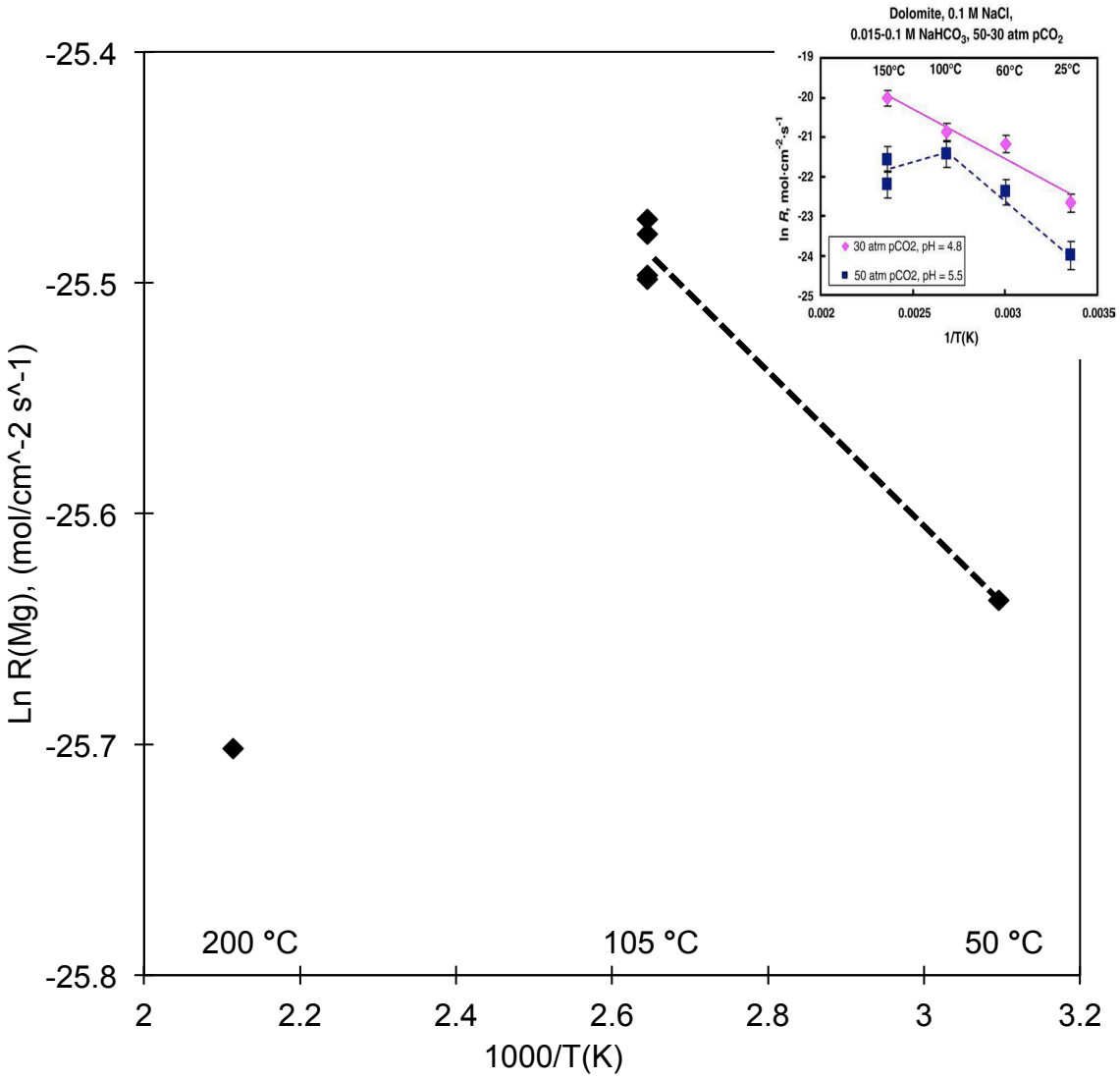
Dolomite, 0.1 M NaCl,
0.015-0.1 M NaHCO3, 50-30 atm pCO2
150°C
100°C
60°C
25°C
ln R, mol·cm^-2·s^-1
30 atm pCO2, pH = 4.8
50 atm pCO2, pH = 5.5
1/T(K)
Ln R(Mg), (mol/cm^-2 s^-1)
200 °C
105 °C
50 °C
1000/T(K)